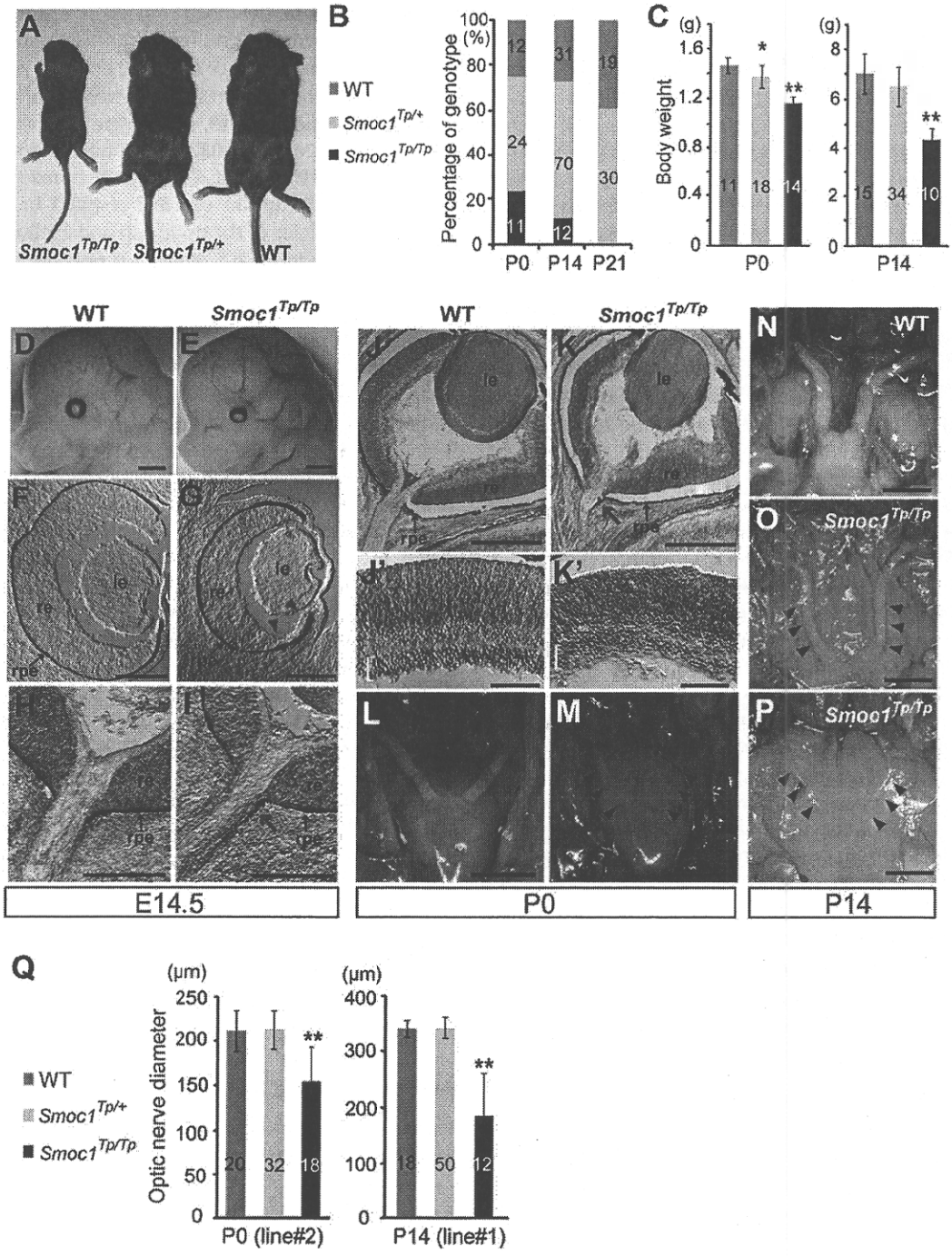

Figure 3. Growth and Ocular Phenotypes of *Smoc1* Null Mice

(A) Representative *Smoc1*$^{Tp/Tp}$ mouse, showing a small body in comparison to *Smoc1*$^{Tp/+}$ and WT littermates.

(B) Genotypes of living pups during the first 3 wk of life.

(C) Body weight of pups of each genotype at P0 (left panel) and P14 (right panel).

(D and E) Relatively small eyes were evident in *Smoc1*$^{Tp/Tp}$ mice in comparison to WT mice.

(F–K′) Coronal sections of eyes at E14.5 (F–I) and P0 (J–K′) with TB staining (H, I, and J–K′). (F-I) Atrophy of the anteroventral part of the retina (G, magenta arrowheads, dorsal view shown at the top), hypoplastic optic nerve, and extension of the RPE to the optic nerve (I, magenta arrow) in *Smoc1*$^{Tp/Tp}$ mice at E14.5. (J and K) Hypoplastic optic nerve and RPE extension in *Smoc1*$^{Tp/Tp}$ mice at P0 (K, magenta arrow). Note that sections in which optic nerves appeared most thick are presented in (H–K). (J′–K′) In higher-magnification views of (J and K), a thinned and irregular ganglion cell layer (white brackets) was observed in *Smoc1*$^{Tp/Tp}$ mice. Abbreviations are as follows: le, lens; re, retina; rpe, retinal pigmented epithelium.

(L–P) Ventral views of the brain showing optic nerves at P0 (L and M) and P14 (N–P), showing various degrees of optic nerve hypoplasia.

Discussion

In a previous report, we performed parametric linkage analysis with three families (families A, B, and C) and found 16 loci showing a LOD score ($\theta = 0.000$) higher than 3.0. Additional microsatellite markers highlighted only one locus, 10p11.23.[12] However, no mutations were found in the candidate gene *MPP7*.[12] By recruiting a new family (family X) to this study, we successfully found homozygous mutations in *SMOC1* in families A, C, and X. In family B, no *SMOC1* mutations were found, indicating the genetic heterogeneity in MLA. Patients with *SMOC1* mutations and *Smoc1* null mice showed similar limb anomalies, such as oligodactyly, syndactyly, synostosis of 4th and 5th metacarpals, hypoplasia of fibula, and bowed tibia. Oligodactyly, syndactyly, and synostosis of 4th and 5th metacarpals are common in MLA patients.[2–4] However, hypoplastic fibula and bowed tibia are less common in patients with MLA, as four out of 34 MLA patients showed these anomalies in the previous report.[3] Although one patient with a *SMOC1* mutation from family C did not show bowed tibia and hypoplastic fibula, these anomalies could be features specific to *SMOC1* mutations. Further *SMOC1* analysis of other MLA patients should delineate the phenotypic consequences caused by *SMOC1* mutations.

Accumulating evidence suggests that BMP signaling plays crucial roles in early eye vesicle and limb patterning, skeletal formation, and apoptosis of the interdigital mesenchyme,[25–29] and mutations involving BMP signaling cause human malformations including ocular, limb, and skeletal anomalies.[7,30–33] Here, we present genetic evidence that *SMOC1* is essential for ocular and limb development in humans and mice. Furthermore, *Xenopus smoc* can inhibit BMP signaling,[11] suggesting that *SMOC1/Smoc1* can also modulate BMP signaling in humans and mice. Indeed, we observed reduced and/or disturbed expression of genes involved in BMP signaling in the interdigital mesenchyme in *Smoc1* null mice, and limb and ocular abnormalities associated with loss of *Smoc1* function are consistent with phenotypic consequences of disturbed BMP signaling. Conditional inactivation of *Bmp2* in the limb showed 3/4 syndactyly, and a similar deficiency of both *Bmp2* and *Bmp7* resulted in malformed fibulae in mice.[25] Moreover, mice deficient in *Fmn1*, a repressor of BMP signaling, showed four digits, fused metatarsal bones, and an absence of fibulae in the hindlimbs,[34] suggesting the importance of altered BMP signaling in these features. Concerning ocular phenotypes, haploinsufficiency of mouse *Bmp4* resulted in a decreased number of ganglion layer cells and absence of the optic nerve similar to *Smoc1* null mice,[35] indicating that altered BMP signaling is also involved in the ocular phenotype. Interestingly, knockdown experiments of *smoc* by antisense morpholino in *Xenopus* showed absence or severe deformity of the eye and other anterior structures, which were accompanied by aberrant expression of *otx2*, *tbx2* in the eye field.[11] Mutations of *OTX2* (MIM 600037) cause micropthalmia, syndromic 5 (MCOPS5 [MIM 610125]) in humans.[36] Moreover, targeted disruption of *Tbx2* resulted in a marked reduction in the size of the optic cup and a failure of optic nerve formation in mice.[37] Thus, it is possible that loss of *SMOC1* function could alter the expression of *OTX2* and *TBX2* (MIM 600747) by disturbing BMP signaling in human developing eyes.

It is unknown how the loss of functional SMOC1, a BMP antagonist, leads to reduced expression of genes involved in BMP signaling in the interdigital mesenchyme in *Smoc1* null mice. In the case of *Fmn1*-deficient mice, the loss of the repressor of BMP signaling resulted in downregulation of *Fgf4* and *Shh* and in upregulation of *Gremlin* expression at E10.5, and absence of apoptosis of the interdigital mesenchyme between the two middle digits at E13.5.[34] Thus, there is a possibility that loss of SMOC1 could cause the imbalance among BMP, SHH, and FGF signaling, which would subsequently lead to reduced and/or disturbed expression of genes involved in BMP signaling in the interdigital mesenchyme. In fact, we observed reduced expression of *Msx2* in the progressive zone of hindlimbs at E11.5 (Figure S2). Moreover, expression of *Sox9*, the initial cartilage condensation marker, showed abnormal limb patterning, suggesting that SMOC1 may affect BMP signaling even at early stages of limb development (Figure S3). Further examinations are required for understanding spatial and temporal actions of SMOC1/Smoc1 protein during limb development.

In conclusion, our data demonstrate that *SMOC1/Smoc1* is an essential player in both ocular and limb development in humans and mice and give further support to the crucial roles of BMP signaling in these systems.

Supplemental Data

Supplemental Data include three figures and four tables and can be found with this article online at http://www.cell.com/AJHG/.

Acknowledgments

We would like to thank the patients and their families for their participation in this study. We thank Yoshiko Takahashi (Nara Institute of Science and Technology) and Atsushi Yamada (Showa University) for providing the *Bmp2* and *Sox9* probes; Elizabeth J. Robertson (University of Oxford) and Makoto Ishibashi (Kyoto University) for the *Bmp7* probe; Robert E. Maxson, Jr. (University of Southern California Keck School of Medicine) for the *Msx2*

(Q) Optic nerve diameter. Optic nerves were significantly hypoplastic in $Smoc1^{Tp/Tp}$ mice in comparison to WT and $Smoc1^{Tp/+}$ littermates. The numbers of pups (B and C) or eyes (Q) corresponding to each genotype are indicated within bars. Error bars indicate standard deviation: *$p < 0.01$, compared with WT. **$p < 0.01$, compared with WT and $Smoc1^{Tp/+}$. Scale bars represent 1 mm (D, E, and L–P), 200 μm (F–I), 500 μm (J and K), and 100 μm (J′ and K′).

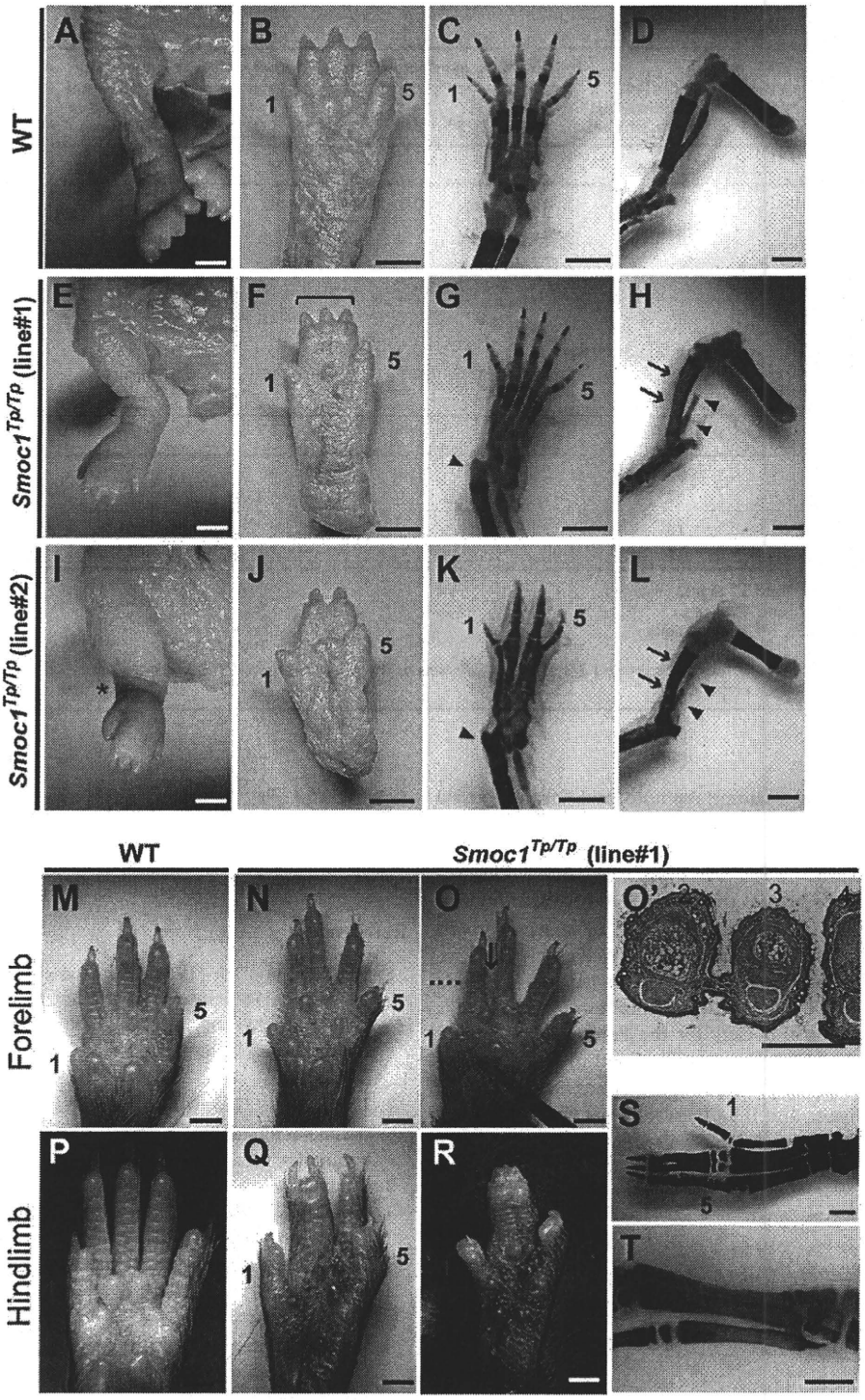

Figure 4. Limb Phenotypes of *Smoc1* Null Mice

Limbs of WT (A–D, M, and P) and *Smoc1*$^{Tp/Tp}$ mice (E–L, N–O′, and Q–T) at P0 (A–L) and P14 (M–T). Digit identities are indicated by the numbers 1 (thumb, anterior) and 5 (little finger, posterior). Skeletal staining with alcian blue and alizarin red is presented (C, D, G, H, K, L, S, and T). *Smoc1*$^{Tp/Tp}$ mice showed pes valgus (E and I), soft tissue syndactyly (F and G), and four digits with metatarsal fusion (J and K). Malposition of the articulation between the tibia/fibula and the calcanea (G and K, magenta arrowheads), bowed tibia (magenta arrows), and hypoplastic fibula (arrowheads) of *Smoc1*$^{Tp/Tp}$ mice (H and L) were observed. 2/3 soft tissue syndactyly (N) and 2/3 webbing (O) were evident in forelimbs of *Smoc1*$^{Tp/Tp}$ mice. (O′) A transverse section taken at the level indicated by the dashed line in (O) showed 2/3 webbing. 2/3 syndactyly (Q), 2/3/4 syndactyly (R), synostosis between the 2nd and 3rd proximal phalanx and metatarsals (S), and synostosis between the 4th and 5th metatarsals (T, arrow), observed in the hindlimbs of *Smoc1*$^{Tp/Tp}$ mice. Scale bars represent 1 mm (A–O and P–T) or 500 μm (O′).

Table 1. Limb Abnormalities in *Smoc1*$^{Tp/Tp}$ Mutants

Genotype	Talipes Valgus (No. of Affected/ Total No. of Pups)	Forelimb Abnormalities (No. of Limbs)	Hindlimb Syndactyly (No. of Limbs)					Other External Abnormalities (No. of Pups)	4th and 5th Metatarsal Fusion (No. of Affected/Total No. of Limbs)
			None	2/3[a]	3/4[b]	2/3/4[c]	4 Digits		
Postnatal Day 0									
Smoc1$^{Tp/+}$ (line 1, C57BL/6J)	0/42	0	84	0	0	0	0		
Smoc1$^{Tp/+}$ (line 2, ICR mixed)	0/38	0	76	0	0	0	0		
Smoc1$^{Tp/Tp}$ (line 1, C57BL/6J)	10/10	0	3	0	3	12	2		
Smoc1$^{Tp/Tp}$ (line 2, ICR mixed)	13/17	1[d]	1	1	9	4	19	cleft palate (3)	
Postnatal Day 14									
Smoc1$^{Tp/+}$ (line 1, C57BL/6J)	0/70	0	140	0	0	0	0		
Smoc1$^{Tp/Tp}$ (line 1, C57BL/6J)	11/11	18[e]	2	7	3	8	2	hypoplastic thumbs (5)	9/10[f]

[a] Syndactyly between the 2nd and 3rd digits.
[b] Syndactyly between the 3rd and 4th digits.
[c] Syndactyly between the 2nd, 3rd, and 4th digits.
[d] 2/3 soft tissue syndactyly.
[e] Eleven limbs showed 2/3 webbing, four limbs showed 2/3 soft tissue syndactyly, and one limb showed 3/4 syndactyly.
[f] Based on examination of skeletal preparations.

probe; Tomonori Hirose, Kazunori Akimoto, and Kazunori Sasaki (Yokohama City University) for providing useful information about mouse breeding, taking photos on a stereo microscope, and mRNA quantification; and Kohei Shiota and Sumiko Kimura (Kyoto University) for helpful comments about NB staining and limb anomalies. This work was supported by research grants from the Ministry of Health, Labour and Welfare (T. Furuichi, N. Miyake, N. Matsumoto, and H.S.) and the Japan Science and Technology Agency (N. Matsumoto), a Grant-in-Aid for Scientific Research from the Japan Society for the Promotion of Science (T. Furuichi and N. Matsumoto), and a Grant-in-Aid for Young Scientist from the Japan Society for the Promotion of Science (K.N., H.D., N. Miyake, and H.S.). This work has been carried out at the Advanced Medical Research Center of Yokohama City University.

Received: September 29, 2010
Revised: November 20, 2010
Accepted: November 26, 2010
Published online: December 30, 2010

Web Resources

The URLs for data presented herein are as follows:

BDGP, http://www.fruitfly.org/
ESEfinder 3.0, http://rulai.cshl.edu/cgi-bin/tools/ESE3/esefinder.cgi?process=home
GenBank, http://www.ncbi.nlm.nih.gov/Genbank/
HSF2.4.1, http://www.umd.be/HSF/
NetGene2, http://www.cbs.dtu.dk/services/NetGene2/
Online Mendelian Inheritance in Man, http://www.ncbi.nlm.nih.gov/Omim
UCSC Genome Browser, http://genome.ucsc.edu/cgi-bin/hgGateway
SpliceView, http://zeus2.itb.cnr.it/~webgene/wwwspliceview.html

References

1. Waardenburg, P.J. (1961). Autosomally-recessive anophthalmia with malformations of the hands and feet. In Genetics and Ophthalmology, P.J. Waardenburg, A. Franceschetti, and D. Klein, eds. (Assen, The Netherlands: Royal Van Gorcum), p. 773.
2. Teiber, M.L., Garrido, J.A., and Barreiro, C.Z. (2007). Ophthalmo-acromelic syndrome: report of a case with vertebral anomalies. Am. J. Med. Genet. A. *143A*, 2460–2462.
3. Garavelli, L., Pedori, S., Dal Zotto, R., Franchi, F., Marinelli, M., Croci, G.F., Bellato, S., Ammenti, A., Virdis, R., Banchini, G., and Superti-Furga, A. (2006). Anophthalmos with limb anomalies (Waardenburg opththalmo-acromelic syndrome): report of a new Italian case with renal anomaly and review. Genet. Couns. *17*, 449–455.
4. Tekin, M., Tutar, E., Arsan, S., Atay, G., and Bodurtha, J. (2000). Ophthalmo-acromelic syndrome: report and review. Am. J. Med. Genet. *90*, 150–154.
5. Adler, R., and Canto-Soler, M.V. (2007). Molecular mechanisms of optic vesicle development: complexities, ambiguities and controversies. Dev. Biol. *305*, 1–13.
6. Zeller, R., López-Ríos, J., and Zuniga, A. (2009). Vertebrate limb bud development: moving towards integrative analysis of organogenesis. Nat. Rev. Genet. *10*, 845–858.
7. Bakrania, P., Efthymiou, M., Klein, J.C., Salt, A., Bunyan, D.J., Wyatt, A., Ponting, C.P., Martin, A., Williams, S., Lindley, V., et al. (2008). Mutations in BMP4 cause eye, brain, and digit

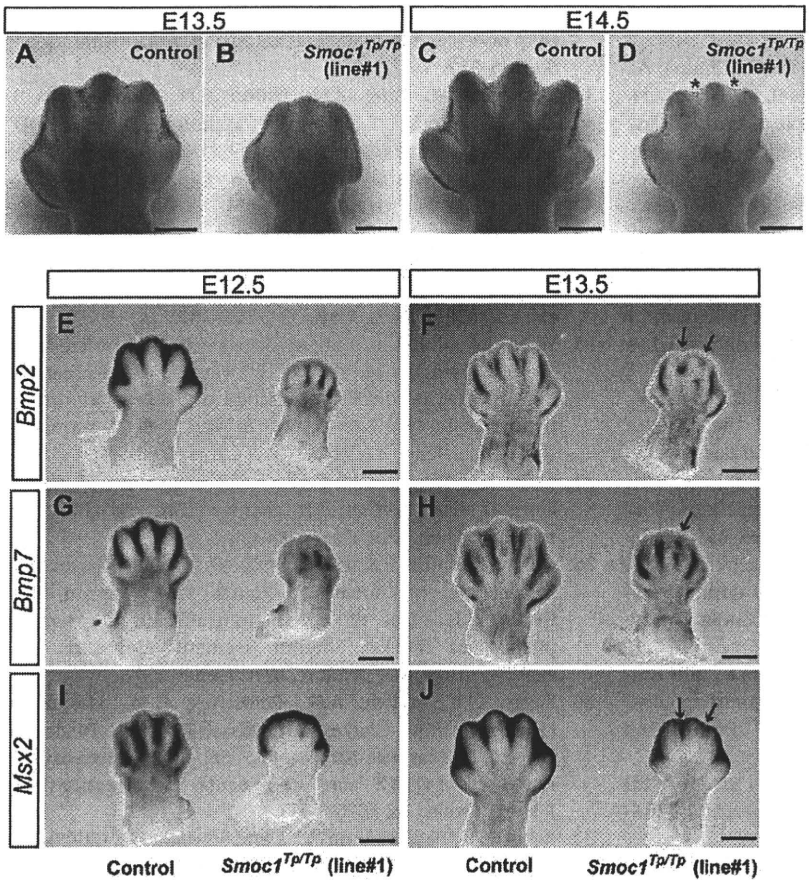

Figure 5. Reduced Apoptosis and Altered BMP Signaling in the Interdigital Mesenchyme of *Smoc1* Null Mice

(A–D) NB staining of left hindlimbs at E13.5 (A and B) and E14.5 (C and D). In comparison to control embryos (WT and $Smoc1^{Tp/+}$ littermates) (A and C), the number of NB-stained apoptotic cells in the interdigital mesenchyme of $Smoc1^{Tp/Tp}$ mice was dramatically reduced between digits 2 and 3 and digits 3 and 4 at both E13.5 and E14.5, and the webbing remained at a distal level (B and D, magenta asterisk).

(E–J) Whole-mount in situ hybridization of right hindlimbs at E12.5 (E, G, and I) and E13.5 (F, H, and J). At E12.5, interdigital expression of *Bmp2*, *Bmp7*, and *Msx2* was profoundly delayed in the hindlimbs of $Smoc1^{Tp/Tp}$ mice, and their expression in the interdigital mesenchyme was apparently perturbed, even at E13.5 (magenta arrows). Scale bar represents 500 μm.

developmental anomalies: overlap between the BMP4 and hedgehog signaling pathways. Am. J. Hum. Genet. *82*, 304–319.

8. Bornstein, P., and Sage, E.H. (2002). Matricellular proteins: extracellular modulators of cell function. Curr. Opin. Cell Biol. *14*, 608–616.
9. Vannahme, C., Smyth, N., Miosge, N., Gösling, S., Frie, C., Paulsson, M., Maurer, P., and Hartmann, U. (2002). Characterization of SMOC-1, a novel modular calcium-binding protein in basement membranes. J. Biol. Chem. *277*, 37977–37986.
10. Gersdorff, N., Müller, M., Schall, A., and Miosge, N. (2006). Secreted modular calcium-binding protein-1 localization during mouse embryogenesis. Histochem. Cell Biol. *126*, 705–712.
11. Thomas, J.T., Canelos, P., Luyten, F.P., and Moos, M., Jr. (2009). Xenopus SMOC-1 inhibits BMP signaling downstream of receptor binding and is essential for post-gastrulation development in Xenopus. J. Biol. Chem. *284*, 18994–19005.
12. Hamanoue, H., Megarbane, A., Tohma, T., Nishimura, A., Miz-uguchi, T., Saitsu, H., Sakai, H., Miura, S., Toda, T., Miyake, N., et al. (2009). A locus for ophthalmo-acromelic syndrome mapped to 10p11.23. Am. J. Med. Genet. A. *149A*, 336–342.
13. Mégarbané, A., Souraty, N., and Tamraz, J. (1998). Ophthalmo-acromelic syndrome (Waardenburg) with split hand and polydactyly. Genet. Couns. *9*, 195–199.
14. Cogulu, O., Ozkinay, F., Gündüz, C., Sapmaz, G., and Ozkinay, C. (2000). Waardenburg anophthalmia syndrome: report and review. Am. J. Med. Genet. *90*, 173–174.
15. Miyake, N., Kosho, T., Mizumoto, S., Furuichi, T., Hatamochi, A., Nagashima, Y., Arai, E., Takahashi, K., Kawamura, R., Wakui, K., et al. (2010). Loss-of-function mutations of CHST14 in a new type of Ehlers-Danlos syndrome. Hum. Mutat. *31*, 966–974.
16. Gudbjartsson, D.F., Thorvaldsson, T., Kong, A., Gunnarsson, G., and Ingolfsdottir, A. (2005). Allegro version 2. Nat. Genet. *37*, 1015–1016.
17. Keng, V.W., Yae, K., Hayakawa, T., Mizuno, S., Uno, Y., Yusa, K., Kokubu, C., Kinoshita, T., Akagi, K., Jenkins, N.A., et al. (2005). Region-specific saturation germline mutagenesis in mice using the Sleeping Beauty transposon system. Nat. Methods *2*, 763–769.
18. Mamo, S., Gal, A.B., Bodo, S., and Dinnyes, A. (2007). Quantitative evaluation and selection of reference genes in mouse oocytes and embryos cultured in vivo and in vitro. BMC Dev. Biol. *7*, 14.
19. Parr, B.A., Shea, M.J., Vassileva, G., and McMahon, A.P. (1993). Mouse Wnt genes exhibit discrete domains of expression in the early embryonic CNS and limb buds. Development *119*, 247–261.
20. Saitsu, H., Ishibashi, M., Nakano, H., and Shiota, K. (2003). Spatial and temporal expression of folate-binding protein 1 (Fbp1) is closely associated with anterior neural tube closure in mice. Dev. Dyn. *226*, 112–117.
21. Tamplin, O.J., Kinzel, D., Cox, B.J., Bell, C.E., Rossant, J., and Lickert, H. (2008). Microarray analysis of Foxa2 mutant mouse embryos reveals novel gene expression and inductive roles

for the gastrula organizer and its derivatives. BMC Genomics *9*, 511.

22. Suzuki, D., Yamada, A., Amano, T., Yasuhara, R., Kimura, A., Sakahara, M., Tsumaki, N., Takeda, S., Tamura, M., Nakamura, M., et al. (2009). Essential mesenchymal role of small GTPase Rac1 in interdigital programmed cell death during limb development. Dev. Biol. *335*, 396–406.
23. Kimura, S., and Shiota, K. (1996). Sequential changes of programmed cell death in developing fetal mouse limbs and its possible roles in limb morphogenesis. J. Morphol. *229*, 337–346.
24. Sernagor, E., Eglen, S.J., and Wong, R.O. (2001). Development of retinal ganglion cell structure and function. Prog. Retin. Eye Res. *20*, 139–174.
25. Bandyopadhyay, A., Tsuji, K., Cox, K., Harfe, B.D., Rosen, V., and Tabin, C.J. (2006). Genetic analysis of the roles of BMP2, BMP4, and BMP7 in limb patterning and skeletogenesis. PLoS Genet. *2*, e216.
26. Robert, B. (2007). Bone morphogenetic protein signaling in limb outgrowth and patterning. Dev. Growth Differ. *49*, 455–468.
27. Dudley, A.T., Lyons, K.M., and Robertson, E.J. (1995). A requirement for bone morphogenetic protein-7 during development of the mammalian kidney and eye. Genes Dev. *9*, 2795–2807.
28. Khokha, M.K., Hsu, D., Brunet, L.J., Dionne, M.S., and Harland, R.M. (2003). Gremlin is the BMP antagonist required for maintenance of Shh and Fgf signals during limb patterning. Nat. Genet. *34*, 303–307.
29. Furuta, Y., and Hogan, B.L. (1998). BMP4 is essential for lens induction in the mouse embryo. Genes Dev. *12*, 3764–3775.
30. Asai-Coakwell, M., French, C.R., Berry, K.M., Ye, M., Koss, R., Somerville, M., Mueller, R., van Heyningen, V., Waskiewicz, A.J., and Lehmann, O.J. (2007). GDF6, a novel locus for a spectrum of ocular developmental anomalies. Am. J. Hum. Genet. *80*, 306–315.
31. Tassabehji, M., Fang, Z.M., Hilton, E.N., McGaughran, J., Zhao, Z., de Bock, C.E., Howard, E., Malass, M., Donnai, D., Diwan, A., et al. (2008). Mutations in GDF6 are associated with vertebral segmentation defects in Klippel-Feil syndrome. Hum. Mutat. *29*, 1017–1027.
32. Wyatt, A.W., Osborne, R.J., Stewart, H., and Ragge, N.K. (2010). Bone morphogenetic protein 7 (BMP7) mutations are associated with variable ocular, brain, ear, palate, and skeletal anomalies. Hum. Mutat. *31*, 781–787.
33. Ye, M., Berry-Wynne, K.M., Asai-Coakwell, M., Sundaresan, P., Footz, T., French, C.R., Abitbol, M., Fleisch, V.C., Corbett, N., Allison, W.T., et al. (2010). Mutation of the bone morphogenetic protein GDF3 causes ocular and skeletal anomalies. Hum. Mol. Genet. *19*, 287–298.
34. Zhou, F., Leder, P., Zuniga, A., and Dettenhofer, M. (2009). Formin1 disruption confers oligodactylism and alters Bmp signaling. Hum. Mol. Genet. *18*, 2472–2482.
35. Chang, B., Smith, R.S., Peters, M., Savinova, O.V., Hawes, N.L., Zabaleta, A., Nusinowitz, S., Martin, J.E., Davisson, M.L., Cepko, C.L., et al. (2001). Haploinsufficient Bmp4 ocular phenotypes include anterior segment dysgenesis with elevated intraocular pressure. BMC Genet. *2*, 18.
36. Ragge, N.K., Brown, A.G., Poloschek, C.M., Lorenz, B., Henderson, R.A., Clarke, M.P., Russell-Eggitt, I., Fielder, A., Gerrelli, D., Martinez-Barbera, J.P., et al. (2005). Heterozygous mutations of OTX2 cause severe ocular malformations. Am. J. Hum. Genet. *76*, 1008–1022.
37. Behesti, H., Papaioannou, V.E., and Sowden, J.C. (2009). Loss of Tbx2 delays optic vesicle invagination leading to small optic cups. Dev. Biol. *333*, 360–372.

Birth Defects Research (Part A) 88:487–496 (2010)

Rudimentary Claws and Pigmented Nail-like Structures on the Distal Tips of the Digits of *Wnt7a* Mutant Mice: *Wnt7a* Suppresses Nail-like Structure Development in Mice

Sumiko Kimura,[1*] Hirotomo Saitsu,[2] Blanka A. Schaumann,[3] Kohei Shiota,[1,4] Naomichi Matsumoto,[2] and Makoto Ishibashi[5]

[1]Congenital Anomaly Research center, Graduate School of Medicine, Kyoto University, Kyoto, Japan
[2]Department of Human Genetics, Yokohama City University Graduate School of Medicine, Yokohama, Japan
[3]1580 NW 102 Avenue, Portland, Oregon
[4]Department of Anatomy and Developmental Biology, Graduate School of Medicine, Kyoto University, Kyoto, Japan
[5]Department of Physical Therapy, Human Health Science, Faculty of Medicine, Kyoto University, Kyoto, Japan

Received 2 March 2009; Revised 27 January 2010; Accepted 1 February 2010

BACKGROUND: As *Wnt7a* mutant mice exhibit double ventral structures in the digits of autopods, it has been accepted that dorsal-ventral identity in limb development is regulated by the *Wnt7a* signal. The most important evidence for this was the presence of surface pads, typical characteristics of ventral structures, on the dorsal side of digital tips and at the base of digits and their pigmentation. **METHODS:** The morphologic features of the appendages on the distal tips of digits were inspected in the fore- and hindlimbs of mice having a different *Wnt7a* mutation. The digital structures were examined macroscopically and histologically. **RESULTS:** The *Wnt7a* homozygous mutant mice with defects in postaxial digits had rudimentary claws or claws and pigmented nail-like structures, instead of dorsal pads, on the distal digital tips and hairs on the dorsal surface of the digits of fore- and hindlimbs. Furthermore, pigmented ectopic nail-like structures but not pads were also present on the dorsal surface of the base of digits. Double ventral structures were observed in the bones and tendons, excluding pads in digital areas. **CONCLUSIONS:** These findings suggest that *Wnt7a* is not necessarily an exclusive dorsalizing signal to the dorsal ectoderm of the digital areas of autopods. Rather, the *Wnt7a* signal may participate in suppression of the development of pigmented nail-like structures in normal limb development. This means that even rodents, a species lower than primates in the evolution from claws to nails, have molecular potential to develop cutaneous appendages similar to nails at their location. *Birth Defects Research (Part A) 88:487–496, 2010.* © 2010 Wiley-Liss, Inc.

Key words: claws; nail-like structures; pads; *Wnt7a*; mice

INTRODUCTION

As integumentary appendages on the digital tips of autopods (distal limbs), rodents, such as mice and rats, have sharply curved, pointed claws, whereas most primates, including apes and humans, have thin, flat nails. The exceptions to this are some lower primates, e.g., lemurs and marmosets, who exhibit claws and nails on different digits (Kawai et al., 1968; Thorndike, 1968; Soligo and Muller, 1999; Hamrick, 2003). Concerning appendage morphogenesis, a primary claw or nail field initially develops as an epithelial thickening on the dorsal surface of the distal digital tip, which is the first sign of induction of an epithelial appendage (Chapman, 1986). Following this, a transverse groove appears proximal to the epithelial thickening and forms a deep fold as the epithelial matrix expands. The cells of the germinal matrix at the base of the fold later differentiate and proliferate to produce a (superficial) keratinized layer that slowly slides distally over the claw or nail bed and forms

Sumiko Kimura and Hirotomo Saitsu contributed equally to this work.

*Correspondence to: Sumiko Kimura, Congenital Anomaly Research Center, Graduate School of Medicine, Kyoto University, Kyoto 606-8501, Japan.
E-mail: skimura2428@gmail.com

Published online 2 April 2010 in Wiley InterScience (www.interscience.wiley.com).
DOI: 10.1002/bdra.20662

a claw or nail similar in development and structure (Hamrick, 2003).

These appendages are present on the dorsal side of digital tips. Opposite to them, on the ventral side of digital tips and in the distal areas of the palms and soles, are unpigmented, hairless volar pads (Schaumann and Alter, 1976). Well-developed volar pads are found in corresponding areas of rodents (Okajima and Asai, 1985; Kimura et al., 1994; Tsugane and Yasuda, 1995; Hamrick, 2003; Kimura et al., 2005, 2008) and simians (Cummins and Midlo, 1976; Newell-Morris, 1979), both in adults and as early as during intrauterine development (Cummins, 1929; Kimura and Kitagawa, 1986; Kimura and Schaumann, 1988).

Parr and McMahon (1995) reported that *Wnt7a* homozygous mutant mice produced by gene targeting exhibit double ventral structures on the digits of autopods. The most striking evidence for this was the presence of pigmented dorsal pads at the distal digital tips and the base of the digits of the fore- and hindlimbs. In addition to these abnormalities, the dorsal digital surfaces in severe *Wnt7a* mutants lost their hair. Many mutant mice also lacked postaxial digits. These abnormal limb configurations led to the conclusion that dorsal-ventral identity in normal limb development is regulated by the *Wnt7a* signal and that *Wnt7a* is also required for anterior-posterior patterning.

The purpose of the present work was to determine the effects of a different mutation at *Wnt7a* in mice on the development of the fore- and hindlimbs. We inspected integumentary appendages on the dorsal surface of the distal limbs, focusing on irregularities of the distal digital phalanges in *Wnt7a* homozygous mutant mice. In addition, the development of appendages of the distal digital tip and other morphologic features, including the digital bone and tendon configurations, were studied. We discovered a pigmented nail-like structure rather than a pigmented dorsal pad (regarded as such by Parr and McMahon, 1995), an anomaly that is never observed in normal rodents, on the dorsal side of the digital tips of fore- and hindlimbs. The nail-like structure, located in the dorsoproximal portion of a rudimentary or fully developed claw, appeared on both the fore- and hindlimbs of *Wnt7a* homozygous mutant mice. The significance of nail-like structure development in *Wnt7a* homozygous mutant mice and the as yet unknown role of the *Wnt7a* signal in the digital epithelium in normal limb development in mice are discussed.

MATERIALS AND METHODS

In the present study, spontaneous *Wnt7a* mutant mice were identified in a mouse line with a mixed background of C57BL/6 and ICR. Intercrosses between male and female heterozygous mice produced 256 *Wnt7a* mutant mice. Sixty-seven were homozygous, exhibiting limb defects, and the rest were heterozygous and wild-type mice with normal limbs. In addition to the genotypic criteria, we considered the phenotypic criteria of *Wnt7a* mutant mice established by Parr and McMahon (1995): i.e., homozygous mice lacked postaxial digits and had abnormal integumentary appendages on the dorsal surface of their forelimbs, making them easy to distinguish from phenotypically normal (heterozygous and wild-type) mice. All mice were humanely sacrificed at 2–5 months of age, using ether in accordance with the animal care guidelines of Kyoto University; the fore- and hindlimbs were separated from the body proximal to the wrist/ankle and fixed for several days in Bouin's solution. They were then investigated under a microscope, and photographs were taken. The studied morphologic features included the number and configuration of the digits and claws, the appearance of ectopic nail-like structures, and especially the appearance and location of nail-like structures on the distal digital tips.

Histologic Presentation

The forelimbs of 16 fetuses on GD 14–18, of six newborns on day 0 and 2, and two infants on day 12 were fixed overnight in Bouin's solution at 4°C. After dehydration, all forelimbs were embedded in paraffin, and serial sections were made, 7 μm for histologic longitudinal and transverse sections except for longitudinal sections, with 10 μm for infant limbs. The sections were stained with hematoxylin and eosin to demonstrate the development of appendages and to visualize the duplication of digital structures.

Characterization of Genomic Rearrangements

The *Wnt7a* genotype of adults and embryos were determined by polymerase chain reaction (PCR) amplification of genomic DNA from ear and skin tissues, respectively. PCR primers as previously reported (Adamska et al., 2004) were used: *Wnt7a*-F, 5′-GAG CAT CTG CCA TTA GCA AG-3′; *Wnt7a*-R1, 5′-GCA CAG CCA TCT CAT TAG CT-3′; *Wnt7a*-R2, 5′-TGT GCA CTC AAG GCT CTT GA-3′. The *Wnt7a*-F and *Wnt7a*-R2 primers could amplify the mutant allele to produce a 323-bp product but not the wild-type allele. The product size of the wild-type allele by *Wnt7a*-F and *Wnt7a*-R2 primers would be larger than 48 kb and could not be amplified in standard PCR conditions. *Wnt7a*-F and *Wnt7a*-R1 primers amplified only the wild-type allele but not the mutant allele because the *Wnt7a*-R1 primer is located within the deleted sequence. The identity of the genomic deletion interval of the *Wnt7a* mutant mice used in this study and the $Wnt7a^{UM}$ mice developed at the University of Michigan (Adamska et al., 2004) were confirmed by automated fluorescent cycle sequencing of 323-bp PCR fragments amplified with *Wnt7a*-F and *Wnt7a*-R2 primers using genomic DNA of heterozygous mutant as a template. The genomic deletion of mutant mice was also confirmed by Southern hybridization using *Nsi*I- and *Hind*III-digested genomic DNA obtained from liver samples of wild-type, *Wnt7a* heterozygous, or homozygous mutants. Probes were synthesized by PCR DIG probe synthesis kit (Roche, Basel, Switzerland). Primers are as follows: P1-forward, 5′-GGGCCATCATTTGCTTACTG-3′; P1-reverse, 5′-GCCAACACAAGTCACAGCAC′; P2-forward, 5′- GCA TTTCAACAGCCATGGTA-3′; P2-reverse, 5′-ACTGCAGT GAGGTCCTTGGT−3′. Hybridization, washing, and detection of probes were done according to the manufacturer's protocol. Images were captured on FluorChem (Alpha Innotech, San Leandro, CA).

RESULTS

Molecular Characterization of Genomic Rearrangements of Spontaneous *Wnt7a* Mutant Mice

We identified mice lacking postaxial digits and having abnormal integumentary appendages on the dorsal sur-

face of their forelimbs in Rosa26r mice (Soriano, 1999), which were maintained on a mixed background of C57BL/6 and ICR. The Rosa26r mice were originally maintained in a B6D2 background in Chris Wright's laboratory at Vanderbilt University. The limb deformity was observed to be independent of the Rosa26r allele. The limb deformity of these mice was strikingly similar to that of previously reported *Wnt7a* null mice (Parr and McMahon, 1995). PCR amplification of genomic DNA of these mice revealed that these are mutant mice having a deletion of exons 3 and 4 of *Wnt7a* gene (Fig. 1A, data not shown). The deletion interval was similar to the deletion of spontaneous $Wnt7a^{UM}$ mutant mice developed at the University of Michigan on an ICR background (Adamska et al., 2004). Therefore we performed the same genotyping PCR as Adamska et al. (2004). Interestingly, sequence analysis of PCR products amplified with *Wnt7a*-F and *Wnt7a*-R2 primers revealed that the deletion in our spontaneous mutant mice was identical to the deletion in $Wnt7a^{UM}$ (Fig. 1B, D), suggesting that both mutants possess the same mutation, which occurred in a ICR mouse that was an ancestor of both mouse lines. Southern hybridization analysis using a P1 probe detected an aberrant band spanning deletion breakpoints (Fig. 1C, red dots). Moreover, neither P1 nor P2 probes detected the wild-type band in a *Wnt7a* homozygous (−/−) mutant (Fig. 1C, arrows), indicating complete deletion of these genomic region including exons 3 and 4 of *Wnt7a* gene. These molecular data as well as phenotypic similarities led to the conclusion that the mice were very likely null mutants of *Wnt7a*.

Lack of Digits and Presence of Nail-like Structures on the Distal Tips of Digits of Fore- and Hindlimbs in Adult *Wnt7a* Mutant Mice

The total number of digits, of digits with one or two nail-like structures (Figs. 2, 3) at the digital tip, and their frequencies in 67 *Wnt7a* homozygous mutant mice are summarized for each fore- and hindlimb in Table 1. More postaxial digits showed a larger deletion in both fore- and hindlimbs. Loss of postaxial digits occurred with higher frequency in the forelimbs (17.2% in digit IV; 80.6% in digit V) than hindlimbs (3.7% in digit IV; 44.0% in digit V). The percentage of the total number of digits having one or two nail-like structures at the distal digital tip was also higher in the forelimbs (99.8%) than hindlimbs (57.1%). Digit I of the hindlimbs showed by far the lowest frequency (3.7%) of all examined digits.

Morphologic Characteristics of the Fore- and Hindlimbs in *Wnt7a* Mutant Mice

On the ventral view of the forelimbs in normal adult mice (Fig. 2D-v), a large apical pad was present on the distal phalanx of each digit (Fig. 2D-v3 and 4, E-v2 and 3). Interdigital, thenar, and hypothenar pads were seen in marginal (distal) areas of the palm (Fig. 2D-v, E-v). The dorsal digital surface of the distal phalanx bore a sharp, curved claw (Fig. 2D-v3 and 4, E-v2 and 3, E-d). Dorsal skin containing hairs extended conspicuously to the lateral margins of the ventral surface of each digit (Fig. 2D, E). Neither pads nor integumentary thickenings were present on the distal tip or at the base of the digits on the dorsal side of a normal forelimb (Fig. 2E-d). The configurations of hindlimbs (not shown) were nearly identical to forelimbs, except for a retarded thumb on the forelimbs (Fig. 2D-v, E-v).

On the other hand, *Wnt7a* homozygous mutant mice exhibited defects in the postaxial area of the distal limbs and had abnormal appendages on the digital tips, as described below. The forelimb had an extremely reduced apical pad (Fig. 2A-v3, B-v2, -v3, C-v2–4) compared to normal mice (Fig. 2D-v3 and 4, E-v2 and 3). All claws were rudimentary and were located distal to this reduced apical pad (Fig. 2A-v3, -d2, B-v2, -v3, C-v2–4) on the distal tip of the digit. This clearly differed from the claw located on the dorsal side of the digits of normal mice (Fig. 2D-v3 and 4). Although the nail-like structures were thick and varied in size (Fig. 2A–C), they were situated on the dorsal side of the distal phalanges, and their location corresponded to the well-developed claws of normal mice (Fig. 2D, E); most were pigmented and grew over the rudimentary claws (Fig. 2A-d2, v3, B-v2, C-v2–4).

The distal phalanx of the hindlimbs, however, simultaneously displayed a somewhat reduced apical pad on the ventral side (Fig. 3A-2, B-2), a sharp, curved claw on the distal end (Fig. 3B-2, D-2 and 3, D-5, E-2), and a pigmented, well-developed, thick nail-like structure of variable size on the dorsal side of the digit (Fig. 3A-2, B-2, D-5, E-2). A pair of nail-like structures occasionally appeared on the lateral sides of a digit (Fig. 3A-4, C-5). The following features were shared by the fore- and hindlimbs: (1) the relationship among a pad, a rudimentary or fully developed claw, and the nail-like structure was stable in positional order from the ventral to dorsal side of the digit (Fig. 2A-v3, B-v2, A-d2, B-v3, C-v2-4, Fig. 3A-2, B-2). (2) Pigmented ectopic thick nail-like structures of variable size were also present at the base of the digits (Fig. 2A-v, B-v, C-v, A-d, B-d, Fig. 3A–D). (3) The digits exhibited unusual flexion (Fig. 2A-v, B-v, C-v, Fig. 3A-E). (4) A small number of hairs were present on the dorsal side of the digits (Fig. 2A-v3, B-v2, A-d2, B-v3, C-v2-4, Fig. 3A-2, A-4, B-2, C-5, D-2 and 3, D-5, E-2), similar to normal mice (Fig. 2D-v3 and 4, E-v2 and 3, E-d, Fig. 3F-2).

Development of Appendages of Digital Tips in *Wnt7a* Mutant Mice

To demonstrate the relationships between a pad, claw, rudimentary claw, and nail-like structure, longitudinal sections of the digit were studied on GD14–18 and on day 0, 2, and 12 after birth in *Wnt7a* homozygous mutant and normal mouse fetuses, newborns, and infants.

GD14 (Fig. 4A, B, and Their Magnified a-*v*, -*d*, b-*v*, -*d*)

A very slight elevation was discernible on the ventral side of the digital tip in both a homozygous mouse fetus exhibiting a straight digit and a normal fetus exhibiting a slightly bent digit on GD14 (Fig. 4A, B, a-*v*, b-*v*).

GD15 (Fig. 4C, D, c-*p*, -*c*, -*n*, d-*p*, -*c*)

At a similar site to the slight elevation appearing on GD14, an apical pad was clearly visible as a pad eminence in both fetuses (Fig. 4C, D, c-*p*, d-*p*). On the dorsal side of the digital tip, a primary claw field appeared with a slight eminence in the normal fetus (Fig. 4D), and

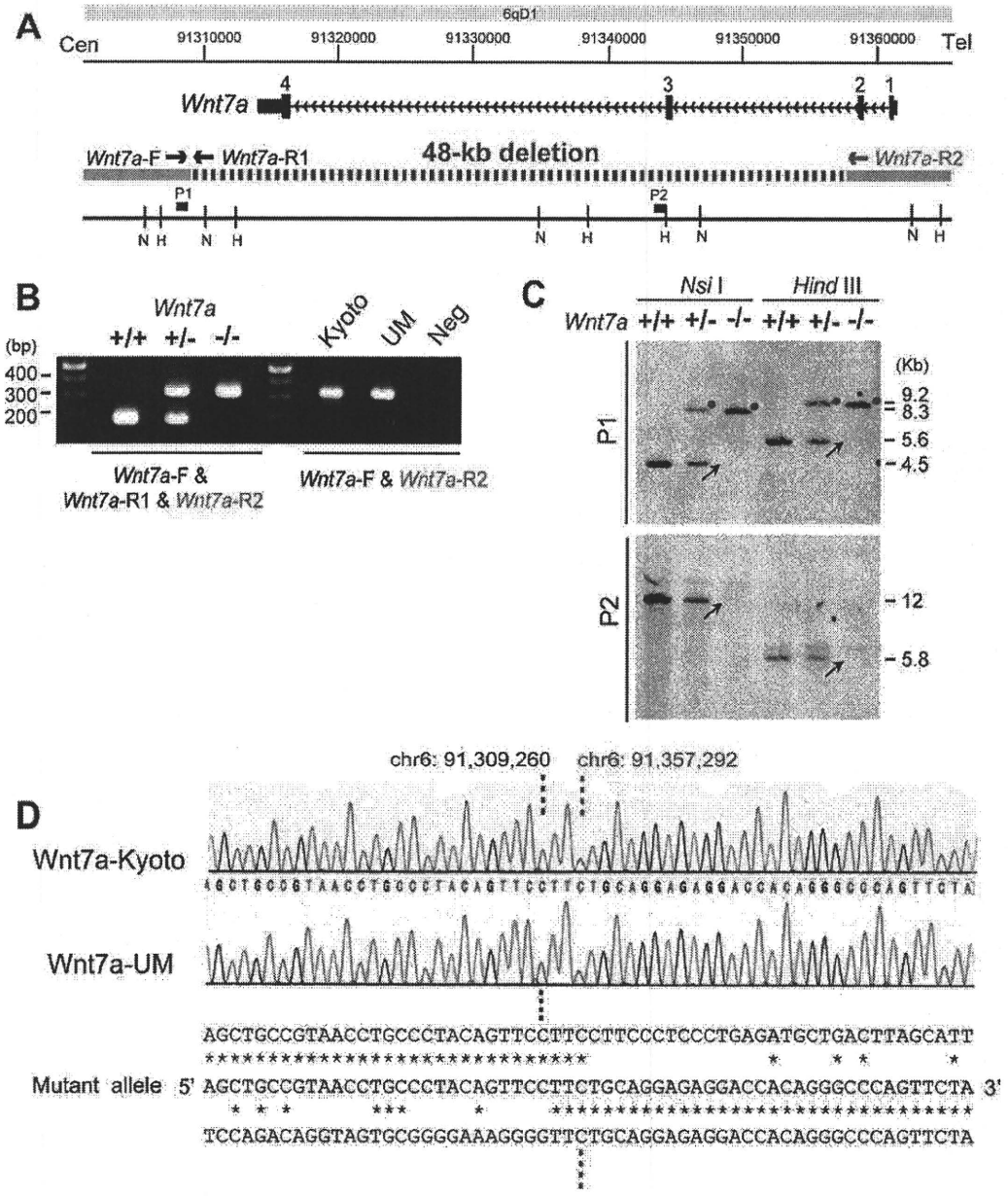

Figure 1. (A) Genomic rearrangements at 6qD1 in *Wnt7a* mutant mice. Top depicts chromosomal bands and genomic location (bp) (Cen, toward the centromere; Tel, toward the telomere); UCSC genome browser coordinate (version July 2007). The deletion (dashed purple line) was 48 kb in size, involving exons 3 and 4 of *Wnt7a*. Intact genomic regions are shown in blue. Primers used for detecting wild-type allele (*Wnt7a*-F and *Wnt7a*-R1) and mutant allele (*Wnt7a*-F and *Wnt7a*-R2) are indicated. Restriction sites (N, *Nsi*I; H, *Hind*III) and probes for Southern hybridization (P1 and P2) are also indicated. Proximal deletion breakpoint and exon 3 of *Wnt7a* are flanked by P1 and P2 probes, respectively. (B) Polymerase chain reaction (PCR) analysis of *Wnt7a* wild-type ($Wnt7a^{+/+}$), heterozygous ($Wnt7a^{+/-}$), and homozygous ($Wnt7a^{-/-}$) mutant mice. Only the 175-bp product from the wild-type allele (lane 2) was observed in wild-type mice, while only the 323-bp product from the mutant allele (lane 4) was observed in homozygous ($Wnt7a^{-/-}$) mutant mice. Both products were observed in heterozygous ($Wnt7a^{+/-}$) mutants (lane 3). Detecting for the mutant allele of both *Wnt7a*-Kyoto and $Wnt7a^{UM}$ mice is shown in lanes 6 and 7, respectively. *Wnt7a*-F and *Wnt7a*-R2 primers successfully amplified identical 323-bp products from both mutant mice. Lanes 1 and 5, size marker; lane 8 (Neg Cont), negative control (no template DNA). Primers used are indicated below. (C) Southern hybridization using probes P1 and P2 on the genomic DNA of *Wnt7a* mutants. Arrows and red dots show normal bands of wild-type allele and aberrant bands specific to the mutant allele, respectively. (D) (Upper) Electropherogram of PCR products from mutant allele (*Wnt7a*-F and *Wnt7a*-R2) revealed that both mutant mice have identical sequence. (Lower) Alignment of deletion junction sequences. Top, middle, and bottom strands show proximal, recombined (mutant), and distal sequences, respectively. Proximal and distal deletion breakpoint locations are marked with black and red dashed lines, respectively. Three nucleotides were overlapped. Asterisks are matched nucleotides in chromosome 6 sequence.

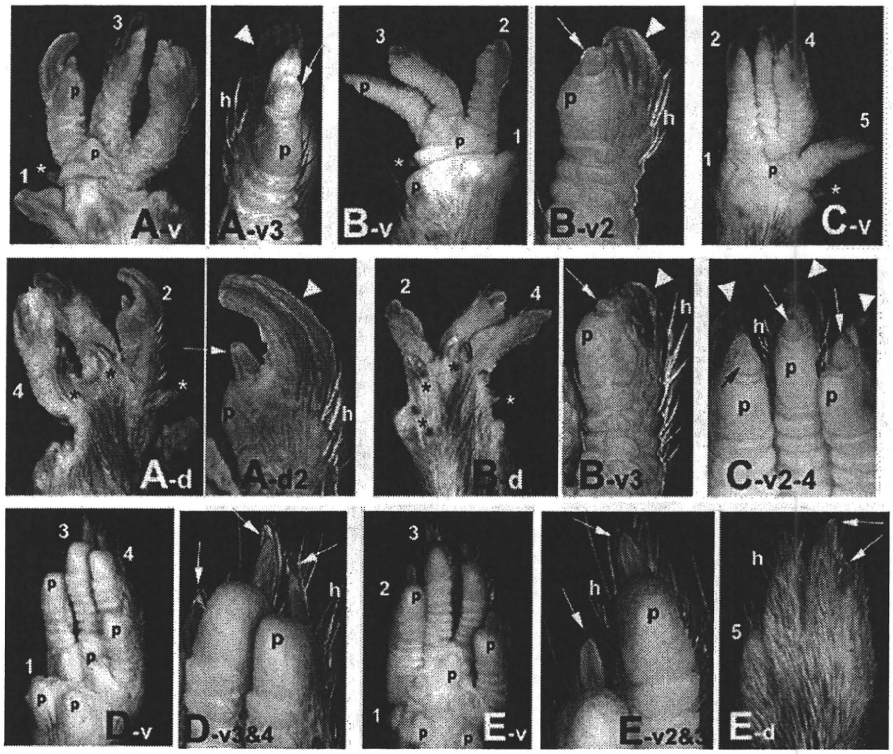

Figure 2. Surface views from the ventral (v) and dorsal (d) sides of the forelimbs in *Wnt7a* homozygous mutant (A–C) and normal (D and E) adult mice. Mutant mice exhibit deficiency in the postaxial portion of the autopods. The autopods in A and B lack digit V. Digit V in C shows abnormal flexion. A truncated claw, indicated by a small arrow, is located at the distal end to the reduced apical pad (A-v3, -d2, B-v2, -v3, C-v2–4; *p*). A pigmented thick nail-like structure, indicated by an arrowhead, appears in the dorsoproximal portion to the truncated claw. A small number of hairs (*h*) are present on the dorsal side of the digits. In normal mice (D, E), a sharp, curved claw is seen on the dorsal side and a well-developed pad on the ventral side of the distal phalanx (D-v3 and 4, Ev2 and 3). The nail-like structure location (A-v3, -d2, B-v2, -v3, C-v2–4; arrowheads) corresponds to that of the well-developed claw (D-v3 and 4, E-v2 and 3; arrows) in normal mice. Pads on the distal digital tips and palmar margins are labeled *p*: ectopic nail-like structures, asterisks: digits, 1–5.

a primary rudimentary claw field was located distal to a nail-like structure field on a dorsal eminence, which is very similar to an apical pad in the homozygous fetus (Fig. 4C).

GD16 (Fig. 4E, F, e-*p*, -*c*, -*n*, f-*p*, -*c*)

With pad development, an undulation and sweat duct began to appear on the dermal surface of the apical pad in both fetuses (Fig. 4E, F, e-*p*, f-*p*). A hair follicle also started to appear on the dorsal skin (Fig. 4F). A claw was thicker than a rudimentary claw and nail-like structure (Fig. 4E, F, e-*c*, e-*n*, f-*c*). A deep (transverse) claw groove appeared in the proximal portion of the claw in the normal fetus and a shallow (transverse) rudimentary claw groove proximal to the rudimentary claw in the homozygous fetus (Fig. 4E, F, e-*c*, f-*c*). The epithelial cells of the claw, rudimentary claw, and nail-like structure gradually increased in thickness, as shown on GD 15, 16 (Fig. 4C-F, c-*c*, -*n*, d-*c*, e-*c*, -*n*, f-*c*), and 17 (data not shown).

GD18 (Fig. 4G, H, g-*p*, -*c*, -*n*, h-*p*, -*c*)

A few sweat ducts were present in the apical pad of both fetuses but none in the dorsal eminence of the homozygous fetus (Fig. 4G, H, g-*p*, -*n*, h-*p*). A very shallow groove appeared in the nail-like structure area of the distal portion (which corresponds to the middle portion of the distal phalanx) of the dorsal eminence (Fig. 4G, g-*n*). In addition, a shallow distal interphalangeal crease appeared on the dorsal surface between the distal and middle phalanges, and, opposite this crease, a distal interphalangeal (flexion) crease was seen proximal to the apical pad on 16–18 (Fig. 4E, G, e-*n*, g-*n*). The last crease was also present in the normal fetus (Fig. 4F, H). A claw plate was visible in the superficial layer of the claw (Fig. 4H, h-*c*). Opposite plates of the rudimentary claw and nail-like structure had not appeared yet and were observed after birth, as shown on PD12 (Fig. 4L, M).

After Birth (Fig. 4I–N)

In newborn mice, a sharp transverse groove appeared in the proximal portion of the rudimentary claw (Fig. 4I, J). A very shallow groove was also seen in the distal

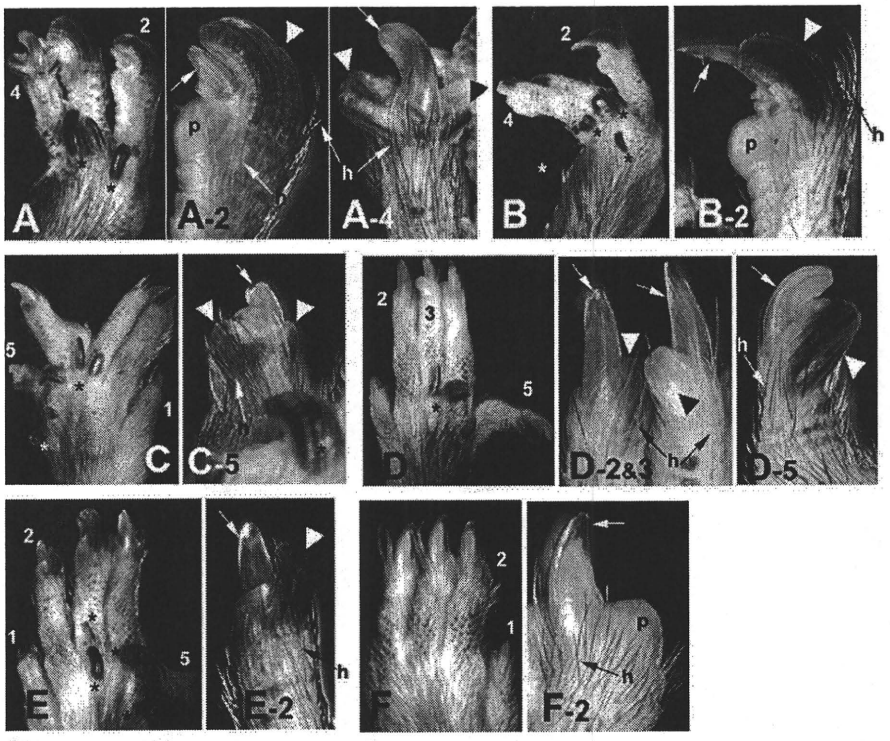

Figure 3. Surface view from the dorsal side of the hindlimbs in *Wnt7a* homozygous mutant (A–E) and normal (F) adult mice. Anomalies include missing (A and B) or shortened (C) digit V and abnormal flexion of digit V (D and E). A thickened nail-like structure (indicated by an arrowhead) is located dorsoproximally to a claw (A-2, B-2, D-2 and 3, D-5, E-2; arrows). A pair of nail-like structures sometimes appears on the dorsolateral sides of a digit (A-4, C-5). Varying degrees of pad regression are seen on the ventral side of a digit with a somewhat reduced claw (A-2). Hairs (*h*) are clearly seen on the dorsal side of the digit with both a claw and a nail-like structure (A-2, 4, B-2, C-5, D-2 and 3, 5, E-2). Ectopic nail-like structures at the base of a digit are indicated by asterisks; digits are labeled 1–5.

portion of the dorsal eminence (Fig. 4I, J). The sweat ducts increased in number on the apical pad but did not appear on the dorsal eminence (Fig. 4I, J). The rudimentary claw slowly reduced in size after birth, and the claw plate grew over the digital tip (Fig. 4K). In infants, the apical pad was filled with sweat ducts and glands in both fetuses (Fig. 4L–N). A short and thin rudimentary claw plate was present on the superficial layer of the rudimentary claw (Fig. 4L). Thick but undeveloped, irregular nail-like structure plates were seen in the distal portion of the dorsal eminence (Fig. 4L, M). In the proximal portion of this eminence, a few sweat ducts (and glands) and dermal ridges were present.

Histologic Digital Configurations of *Wnt7a* Mutant Mice

The configurations of the tendons and bones of digits are shown in longitudinal and transverse (at proximal phalanx level) digital sections of fetal forelimbs at GD16 in *Wnt7a* mutant mice (Fig. 5A–D). The digital configurations of *Wnt7a* homozygous mutant mice (Fig. 5A, C)

Table 1
The total number of digits, of digits with nail-like structures at the digital tip, and their frequencies on the fore- and hindlimbs of 67 *Wnt7a* homozygous mutant adult mice

	Forelimbs (L&R)					Hindlimbs (L&R)					
Digit I	II	III	IV	V	(Total)	I	II	III	IV	V	(Total)
Total number of digits											
134	134	134	111	26	(539)	134	134	134	129	75	(606)
Total number of digits with nail-like structures											
134	134	134	111	25	(538)	5	93	116	65	67	(346)
Percentage of digits with nail-like structures											
100	100	100	100	96.2	(99.8)††	3.7	69.4	86.6	50.4	89.3	(57.1)†

There is no significant difference between fore- (††) and hindlimbs (†) in the percentage of total number of digits with nail-like structures.

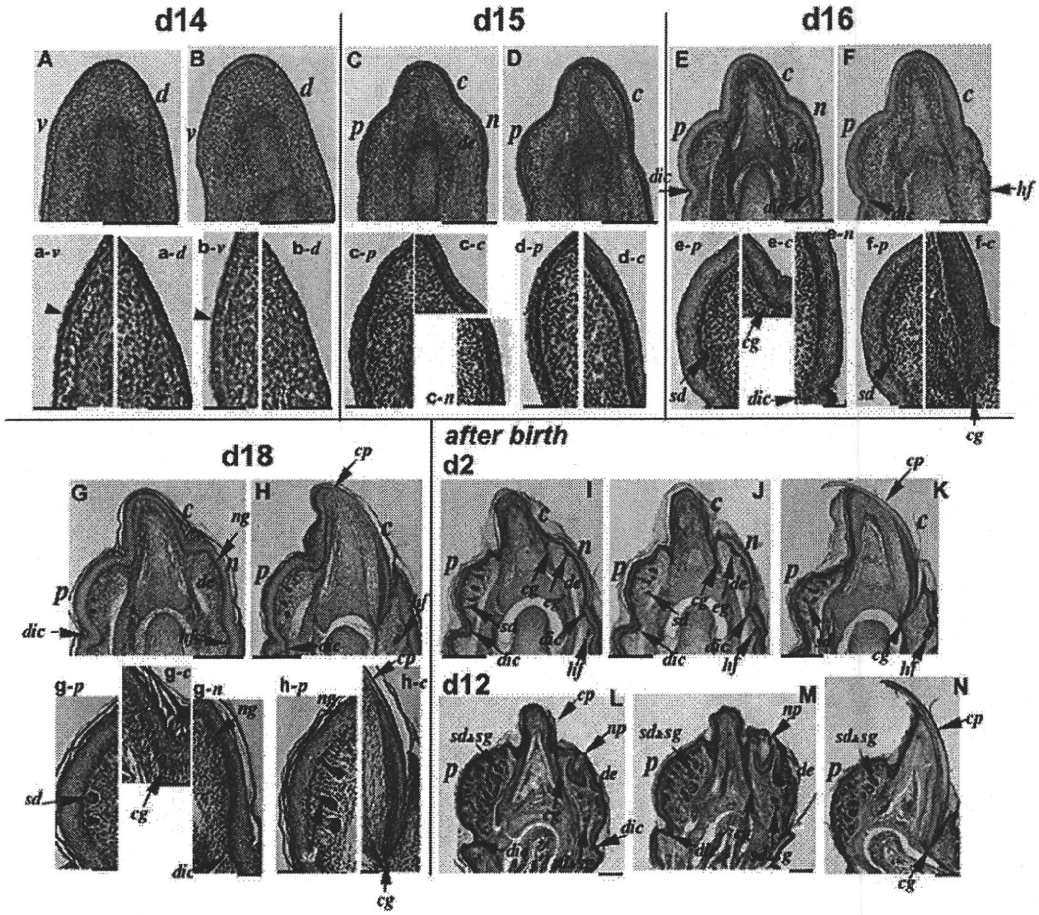

Figure 4. Appendage development in *Wnt7a* homozygous mutant (A, C, E, G, I, J, L, M) and normal (B, D, F, H, K, N) mouse fetuses, newborns, and infants. Longitudinal sections of the distal tips of digits (A–H, upper) and their magnification (a–h, lower) are shown on GD14–16 and 18, and on day 2 (I–K) and 12 (L–N) after birth. On GD14 and 15, a very slight elevation (a-*v*, b-*v*; arrowheads) and an apical pad (C, D; *p*, c-*p*, d-*p*) are visible on the ventral side of the digital tip in both fetuses. On the opposite side, a dorsal eminence (C; *de*) like an apical pad is seen in a homozygous digit. Primary rudimentary claw and nail-like structure fields (C; *c*, *n*) in a homozygous digit are seen on the dorsal side of the digital tip corresponding to the primary claw field (D; *c*) with a slight eminence in the normal digit. With pad development, an undulation and a sweat duct gradually appear on the dermal surface of the apical pad on GD16 (e-*p*, f-*p*; *sd*) in both fetuses. The epithelial cells of the claw, rudimentary claw, and nail-like structure increase in thickness on GD15 and 16 (C-F; *c*, *n*, c-*c*, -*n*, d-*c*, e-*c*, -*n*, f-*c*). A deep claw groove appears at the proximal end of the claw (f-*c*; *cg*) and a shallow rudimentary claw groove proximal to the rudimentary claw (e-*c*; *cg*). On GD18 (G, H), a few sweat ducts are present in the apical pad of both digits (g-*p*, h-*p*; *sd*) but none in the nail-like structure (g-*n*). A claw plate is visible in the superficial layer of the claw (H, h-*c*; *cp*). After birth, a short rudimentary claw groove is present in the proximal portion of the rudimentary claw (I, J; *cg*). There are no sweat ducts in the dorsal eminence (I, J). The nail-like structure slowly increases in thickness with the reduction of the rudimentary claw (I, J, L, M), and the claw plate grows over the digital tip (K; *cp*). In infants, a rudimentary claw plate is discernible at the distal digital tip (L; *cp*) and a thick but undeveloped, irregular nail-like structure plate (L, M; *np*) in the distal portion of the dorsal eminence, respectively. Many sweat ducts and glands are seen on the apical pad in both infants (L, M, N; *p*, *sd* and *sg*) and a few in the proximal portion of the dorsal eminence in homozygous infants (L, M; *de*, *sd* and *sg*). *v*: ventral side; *d*: dorsal side; *de*: dorsal eminence; *ng*: nail-like structure groove; *dic*: distal interphalangeal crease; *hf*: hair follicle. The left side of the digit is the ventral side. Scale bar in A–K 0.2 mm; a–k 0.05 mm.

differed significantly from those of normal mice (Fig. 5B, D). Although the digits of normal mice bent slightly toward the ventral side, this was not the case in *Wnt7a* homozygous mice (Fig. 5A, B), also shown in early stages (Fig. 4A, C). Both sections of *Wnt7a* homozygous mice showed near-mirror images from the midline dividing the ventral and dorsal sides of a digit (Fig. 5A, C). Double ventral configurations were observed in the bones and tendons, excluding pads of digits (Fig. 5A, C and digit I in E). In addition, the configurations of the tendons and bones of the palm are shown in transverse sections at the metacarpal level of forelimbs (Fig. 5E, F). The metacarpals were located on the dorsal side of the limb in normal mice (Fig. 5F) but had shifted in the dorsal direction of the limb in *Wnt7a* homozygous mutant mice (Fig. 5E). No duplication was observed in the metacarpal area of the palm in *Wnt7a* homozygous mice.

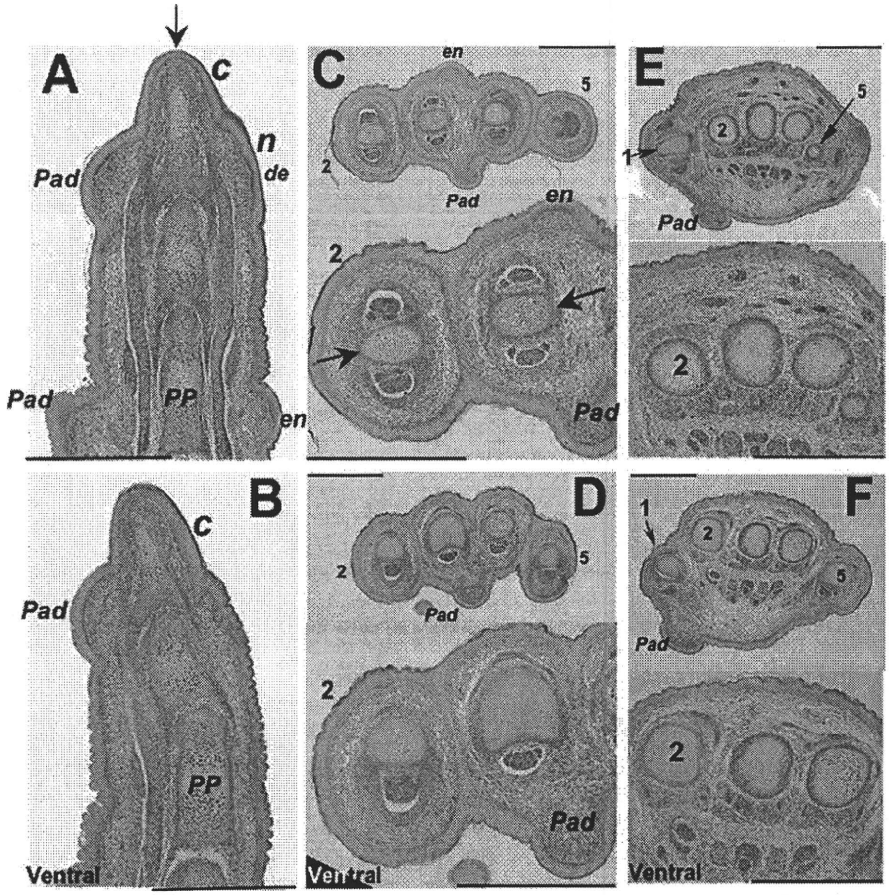

Figure 5. Histologic configurations of digits at GD 16 in *Wnt7a* mutant mouse fetuses. The digit of a normal limb bends slightly toward the ventral side (B); no similar flexion is seen in a mutant limb (A). Longitudinal and transverse sections of mutant fetuses show a mirror-image duplication of tendons and bones (indicated by an arrow) at the phalanx (A, C) but not at the metacarpal level (E). Palmar configurations of the homozygous limb are similar to those of normal mice (E, F), except for a deficiency in the postaxial limb (upper in C and E). A duplicated digit I at the level of the proximal phalanx is seen in E (upper). *c*: claw; *n*: nail-like structure; *de*: dorsal eminence; *pp*: proximal phalanx. Digits are labeled 1, 2, and 5. Scale bar = 0.5 mm.

DISCUSSION

The signaling molecule *Wnt7a*, which is expressed on the dorsal ectoderm of the limb bud, was identified as a regulator of dorsal-ventral patterning in the developing vertebrate limb (Dealy et al., 1993; Parr et al., 1993). In the present study, limb deformities and abnormal digital appendages were inspected in the fore- and hindlimbs of *Wnt7a* homozygous mutant mice lacking the normal Wnt7a function and compared to those reported by Parr and McMahon (1995) and Cygan et al. (1997), as described below.

Larger digital deletion occurred in the more postaxial digits of both the fore- and hindlimbs in *Wnt7a* homozygous mutant mice. These observations correspond to an earlier report (Parr and McMahon, 1995), supporting the conclusion that *Wnt7a* is required for anterior-posterior patterning.

In the forelimbs of *Wnt7a* homozygous mutant mice, rudimentary claws located distal to the reduced apical pads on the digital tip were identical to the truncated nails observed by Parr and McMahon (1995) at the dorsal-ventral interface of digits. They were never located on the dorsal side of the distal digital phalanges as seen in the claws of normal mice. Instead of rudimentary claws, nail-like structures of variable size appeared on the dorsal surface of the distal phalanges of most digits (99.8%), as indicated in Table 1. Their location was similar to that of the well-developed claws of normal mice. In the embryological development of these appendages, a rudimentary claw appeared in the dorso-distal portion of the distal tip of the digit and a nail-like structure in the dorso-proximal section on GD15, respectively. At around birth, the rudimentary claw slowly reduced with the growth of a nail-like structure. As shown in adult mutant mice, most nail-like structures grew over the rudimentary claws and were deeply pigmented. These nail-like structures corresponded to the striations on the dorsal epidermis (Cygan et al., 1997) at the distal tip of the digits, which were originally considered to be dorsal pads (Parr

and McMahon, 1995). In histologic sections, the dorsal eminence containing a nail-like structure in its distal portion was very similar to that of an apical pad on GD15; however, the dorsal eminence did not have any sweat ducts or dermal undulations, unlike the pads of fetuses and newborns. This is evidence that the dorsal eminence is not a pad in structure because it is well known that sweat ducts begin to appear on the pads in intrauterine rodents (Okajima and Asai, 1985; Kimura et al., 1994; Tsugane and Yasuda, 1995). In addition, an apical pad is usually unpigmented, unlike the nail-like structure. A very few ridges, sweat ducts, and the dorsal distal interphalangeal crease were seen in the proximal portion of the dorsal eminence without hairs in infants, which corresponded to the dorsal configuration of the distal phalanx of some primates, including humans.

The claws of the hindlimbs, unlike those of the forelimbs, were nearly normal. This is the first report dealing with the configuration of the claws of the hindlimbs of *Wnt7a* homozygous mutant mice. Interestingly, the hindlimbs simultaneously exhibited a somewhat reduced apical pad on the ventral side, a sharp, curved claw at the distal end, and a pigmented, well-developed nail-like structure of variable size on the dorsal side of the digit. The positional order of these appendages was the same as that of the forelimbs. Although the frequency of a nail-like structure was lower in hindlimbs (57.1%) than in forelimbs (99.8%), as shown in Table 1, the location of nail-like structures corresponded to that of the forelimbs, similar to the claw in normal mice.

A pair of nail-like structures occasionally appeared on the lateral sides of a digit, corresponding to the previously described striations of the dorsal epidermis at the center or on the lateral sides of the distal digital tip in forelimbs (Cygan et al., 1997). In addition, pigmented ectopic nail-like structures of variable size were also present at the base of the digits of both fore- and hindlimbs. Their location was similar to that of the ectopic dorsal pads found previously (Parr and McMahon, 1995; Cygan et al., 1997) but not in our study. Based on the fact that the dorsal pads were pigmented, Parr and McMahon (1995) concluded that the migration of melanocytes is unaffected by *Wnt7a* mutation. A small number of hairs were present on the dorsal side of all digits in *Wnt7a* homozygous mutant mice, similar to normal mice. This is also supported by the appearance of hair follicles in both fetuses. In the previous report (Parr and McMahon, 1995), however, hairs were absent on the dorsal surface of the digits in severe *Wnt7a* mutants.

In longitudinal and transverse sections of the forelimbs, the double ventral configurations in the bones and tendons support the conclusion that *Wnt7a* is required for a dorsalizing signal in the mesenchyme (Parr and McMahon, 1995). *Wnt7a* acts through the *Wnt* coreceptor *Lrp6* to regulate *Lmx1b* expression during dorsal specification in the mouse limb development (Adamska et al., 2005); however, we inferred that *Wnt7a* provides a dorsalizing signal to the mesenchyme but not to the ectoderm in normal limb development, because the pigmented nail-like structures and hairs appeared on the dorsal side of the digits, while duplication occurred only in the bones and tendons of *Wnt7a* homozygous mutant mice lacking normal *Wnt7a* activity. In *En*-1 mutant mice with loss of Engrailed-1 function, which represses the expression of *Wnt7a*, Loomis et al. (1996) reported that ectopic *Wnt7a*, which is expressed in the ventral ectoderm of the distal limb, resulted in dorsal characteristics, such as hair and pigmentation on the ventral skin, and a dorsal pattern of tendon and bone formation in adult *En*-1 mutant limbs. In our study, however, dorsal-to-ventral transformation of ectoderm cell fate does not seem to occur in *Wnt7a* homozygous mutant mice without the Wnt7a function, as hair and pigmentation were normally present on the dorsal skin. Although we cannot account for the discrepancy between the two studies as related to the ectoderm, another, perhaps as yet unknown, gene other than *Wnt7a* may be involved in dorsalizing the ectoderm of the distal limb in *Wnt7a* mutant mice, producing hairs and pigmented nail-like structures on the dorsal skin of *Wnt7a* mutant mice lacking the Wnt7a function.

In addition, transverse sections at the metacarpal level of the forelimb displayed an interesting, as yet unreported, finding. The metacarpals of *Wnt7a* homozygous mutant mice shifted in the dorsal direction of the limb, and their palmar configurations were similar to normal limbs. Even in the hindlimbs of a *Wnt7a* homozygote, the metatarsals were located on the dorsal side (Chen and Johnson, 2002); therefore, no duplication occurred in the metacarpal/metatarsal areas of either the fore- (in our study) or hindlimbs (Chen and Johnson, 2002) in *Wnt7a* homozygous mice with loss of the Wnt7a function. This suggests that the *Wnt7a* signal may be limited to the more distal mesenchyme (future phalangeal portions of the digital areas) of an autopod.

Our spontaneous *Wnt7a* mutants possess the same genomic deletion as $Wnt7a^{UM}$ mice, in which exons 3 and 4 of *Wnt7a* gene were completely deleted. The spontaneous postaxial hemimelia (*px*) mutation has been reported to generate an abnormal splicing event within exon 3 of the *Wnt7a* gene, resulting in a truncated Wnt7a protein (Parr et al., 1998). Morphologic similarities and breeding experiments suggested that the *px* is a likely null allele of the *Wnt7a* gene (Parr et al., 1998). Thus it is very likely that a deletion of exons 3 and 4 of the *Wnt7a* gene resulted in complete loss of Wnt7a function. However, concerning the inconsistencies between the two studies described above, we cannot deny that they may have occurred by different targeting regions of the *Wnt7a* gene; that is, Parr and McMahon (1995) produced a *Wnt7a* mutation by inserting a neomycinresistance (neo) gene into the second exon, while we obtained a spontaneous *Wnt7a* mutation with deletion of the third and fourth exons. In addition, even in animals with a mutation by the same targeting region of the same gene, the animals do not always have exactly the same phenotype. It also remains possible that the first two exons somehow are being joined to exons from another gene to produce a hybrid transcript with some altered Wnt7a protein function.

Hamrick (2001) proposed that different molecules are involved in different stages of the morphogenesis of mammalian distal limb appendages, such as claws and nails, e.g., *Hoxa13* and *Bmp4*, are expressed during condensation formation, *Shh* in the induction of the epithelial fold and germinal epidermal cells, and *Msx*1 and 2 in the growth of the appendage. In addition to these molecules, he stated that *Wnt7a* determines the skin appendage orientation (Hamrick, 2001), as witnessed by the truncated claws in *Wnt7a* homozygous mice lacking normal Wnt7a function (Parr and McMahon, 1995). In our study, how-

ever, the hindlimbs of *Wnt7a* homozygous mice exhibited claws very similar to those of normal mice; therefore, we propose that the *Wnt7a* gene represses the development of nail-like structures rather than determining claw orientation. In a patient with congenital duplication of the palm syndrome (also known as limb/pelvis-hypoplasia/aplasia syndrome) resulting from *Wnt7a* gene mutations, a rudimentary nail was present at the distal digital tip (Al-Qattan et al., 2007). The limb phenotype of this syndrome with individuals lacking all digits of the feet seems to differ from that of *Wnt7a* homozygous mutant mice because loss or reduction of the postaxial digits in *Wnt7a* homozygotes occurs with higher frequency in the forelimbs than hindlimbs (Parr and McMahon, 1995; our present study).

Our observations led to the conclusion that *Wnt7a* does not act as an exclusive dorsalizing signal in the epithelium in normal digital development. This was demonstrated by pigmented nail-like structures and hairs appearing on the dorsal digital side in *Wnt7a* homozygous mutant mice without the Wnt7a function; therefore, the role of *Wnt7a* is not to dorsalize the epithelium, but to suppress nail-like structure development.

This suggests that rodents have the molecular potential to develop pigmented nail-like structures, which had been deemed to be solely a property of primates. This interpretation is also supported by the flat nails found in *Hoxc13* homozygous mutant mice (Godwin and Capecchi, 1998). Furthermore, it suggests that *Wnt7a* might be one of the yet unrecognized genes involved in the evolution from claws to nails. An extinct species, *Carpolestes simpsoni*, one of the earliest primate-like mammals of the late Paleocene, had a grasping foot that shared several features with modern primates, including an opposal big toe with a nail rather than a claw (Sargis, 2002). *Carpolestes* appears to have exhibited an intermediate condition, providing the first evidence of the transition from claws to nails in primates (Sargis, 2002). In *Wnt7a* homozygous mutant mice obtained by spontaneous development not by gene targeting, a truncated, rudimentary, reduced claw and a pigmented nail-like structure appeared at the distal tip of each digit in the forelimbs, suggesting that unknown molecules are involved in the evolution of primate appendages.

ACKNOWLEDGMENTS

We thank Dr. Miriam H. Meisler (University of Michigan) for providing us genomic DNA of the heterozygous *Wnt7a*^{UM} mutant, and Dr. Yoshiya Kawaguchi for providing Rosa26r mice. We also thank Drs. Shigehito Yamada, Toshiya Takigawa, and Lanying Zhao for their technical assistance. This work was supported in part by grants-in-aid from the Japanese Ministry of Education, Science, Sports and Culture.

REFERENCES

Adamska M, Billi AC, Cheek S, et al. 2005. Genetic interaction between *Wnt7a* and *Lrp6* during patterning of dorsal and posterior structures of the mouse limb. Dev Dyn 233(2):368–372.

Adamska M, MacDonald BT, Sarmast ZH, et al. 2004. *En1* and *Wnt7a* interact with *Dkk1* during limb development in the mouse. Dev Biol 272(1):134–144.

Al-Qattan MM, Eyaid W, Al-Balwi M. 2007. Congenital duplication of the palm syndrome. Ann Plast Surg 59(3):341–343.

Chapman RE. 1986. Hair, wool, quill, nail, claw, hoof, and horn. In: Bereiter-Hahn JMA, Richards KS, editors. Biology of the integument. New York: Springer. pp. 293–312.

Chen H, Johnson RL. 2002. Interactions between dorsal-ventral patterning genes *lmx1b*, *engrailed-1* and *wnt-7a* in the vertebrate limb. Int J Dev Biol 46(7):937–941.

Cummins H. 1929. The topographic history of the volar pads (walking pads; Tastballen) in the human embryo. Contrib Embryol 20:103–126.

Cummins H, Midlo C. 1976. Finger prints, palms and soles. South Berlin: Research Publishing Company.

Cygan JA, Johnson RL, McMahon AP. 1997. Novel regulatory interactions revealed by studies of murine limb pattern in *Wnt-7a* and *En-1* mutants. Development 124(24):5021–5032.

Dealy CN, Roth A, Ferrari D, et al. 1993. *Wnt-5a* and *Wnt-7a* are expressed in the developing chick limb bud in a manner suggesting roles in pattern formation along the proximodistal and dorsoventral axes. Mech Dev 43(2–3):175–186.

Godwin AR, Capecchi MR. 1998. Hoxc13 mutant mice lack external hair. Genes Dev 12(1):11–20.

Hamrick MW. 2001. Development and evolution of the mammalian limb: adaptive diversification of nails, hooves, and claws. Evol Dev 3(5): 355–363.

Hamrick MW. 2003. Evolution and development of mammalian limb integumentary structures. J Exp Zool B Mol Dev Evol 298(1):152–163.

Kawai M, Iwamoto M, Yoshiba K. 1968. Monkeys of the world. Tokyo: Mainichi Shuppan. [In Japanese.]

Kimura S, Kitagawa T. 1986. Embryological development of human palmar, plantar, and digital flexion creases. Anat Rec 216(2):191–197.

Kimura S, Schaumann B. 1988. Embryological development and prevalence of thumb flexion creases. Anat Rec 222(1):83–89.

Kimura S, Schaumann BA, Plato CC. 1994. Palmar and plantar pads and flexion creases of the rat (Rattus norvegicus). J Morphol 220(3):237–242.

Kimura S, Schaumann BA, Shiota K. 2005. Ectopic dermal ridge configurations on the interdigital webbings of *Hammertoe* mutant mice (*Hm*): another possible role of programmed cell death in limb development. Birth Defects Res A Clin Mol Teratol 73(2):92–102.

Kimura S, Schaumann BA, Shiota K. 2008. Ectopic dermal ridge configurations on the interdigital webbings and postaxial marginal portion of the hindlimb in *Hammertoe* mutant mice (*Hm*). J Morphol 269(10): 1214–1222.

Loomis CA, Harris E, Michaud J, et al. 1996. The mouse Engrailed-1 gene and ventral limb patterning. Nature 382(6589):360–363.

Newell-Morris L. 1979. Functional considerations of interspecific variation in dermatoglyphic pattern intensity in old world monkeys. In: Wertelecki W, Plato CC, editors. Dermatoglyphics—fifty years later. New York: Alan R. Liss. pp. 765–789.

Okajima M, Asai Y. 1985. Anatomical and microscopic study of the volar dermal ridges of the rat (Rattus norvegicus). Am J Phys Anthropol 67(2):81–88.

Parr BA, Avery EJ, Cygan JA, et al. 1998. The classical mouse mutant postaxial hemimelia results from a mutation in the *Wnt* 7a gene. Dev Biol 202(2):228–234.

Parr BA, McMahon AP. 1995. Dorsalizing signal *Wnt-7a* required for normal polarity of D-V and A-P axes of mouse limb. Nature 374(6520): 350–353.

Parr BA, Shea MJ, Vassileva G, et al. 1993. Mouse *Wnt* genes exhibit discrete domains of expression in the early embryonic CNS and limb buds. Development 119(1):247–261.

Sargis EJ. 2002. Paleontology. Primate origins nailed. Science 298(5598): 1564–1565.

Schaumann B, Alter M. 1976. Dermatoglyphics in medical disorders. New York: Springer.

Soligo C, Muller AE. 1999. Nails and claws in primate evolution. J Hum Evol 36(1):97–114.

Soriano P. 1999. Generalized lacZ expression with the ROSA26 Cre reporter strain. Nat Genet 21(1):70–71.

Thorndike EE. 1968. A microscopic study of the marmoset claw and nail. Am J Phys Anthropol 28(3):247–261.

Tsugane M, Yasuda M. 1995. Dermatoglyphics on volar skin of mice: the normal pattern. Anat Rec 242(2):225–232.

Journal of Human Genetics (2010), 1–5

www.nature.com/jhg

ORIGINAL ARTICLE

Breakpoint determination of X;autosome balanced translocations in four patients with premature ovarian failure

Akira Nishimura-Tadaki[1], Takahito Wada[2], Gul Bano[3], Karen Gough[4], Janet Warner[4], Tomoki Kosho[5], Noriko Ando[6], Haruka Hamanoue[1,7], Hideya Sakakibara[7], Gen Nishimura[8], Yoshinori Tsurusaki[1], Hiroshi Doi[1], Noriko Miyake[1], Keiko Wakui[5], Hirotomo Saitsu[1], Yoshimitsu Fukushima[5], Fumiki Hirahara[7] and Naomichi Matsumoto[1]

Premature ovarian failure (POF) is a disorder characterized by amenorrhea and elevated serum gonadotropins before 40 years of age. As X chromosomal abnormalities are often recognized in POF patients, defects of X-linked gene may contribute to POF. Four cases of POF with t(X;autosome) were genetically analyzed. All the translocation breakpoints were determined at the nucleotide level. Interestingly, *COL4A6* at Xq22.3 encoding collagen type IV alpha 6 was disrupted by the translocation in one case, but in the remaining three cases, breakpoints did not involve any X-linked genes. According to the breakpoint sequences, two translocations had microhomology of a few nucleotides and the other two showed insertion of 3–8 nucleotides with unknown origin, suggesting that non-homologous end-joining is related to the formation of all the translocations.
Journal of Human Genetics advance online publication, 9 December 2010; doi:10.1038/jhg.2010.155

Keywords: *COL4A6*; critical region; non-homologous end-joining; premature ovarian failure; X;autosome translocation

INTRODUCTION

Premature ovarian failure (POF) is a disorder characterized by amenorrhea and elevated serum gonadotropins before 40 years of age. The risk of this disorder or natural menopause before 40 years is approximately 1% of women.[1] Heterogeneous etiology should be involved in POF, such as environmental, autoimmune and genetic factors. X chromosomal abnormalities (partial monosomies and X;autosome-balanced translocations) are often observed in POF patients. These rearrangements cluster at Xq13–q26 called the critical region (for POF).[2,3] The critical region is separated into two: critical region 1 at Xq13–q21 and critical region 2 at Xq23–q26.[2,4] It was suggested that several X-linked loci expressing on both X chromosomes, which were required in a higher dosage for normal ovarian function, were involved in POF.[5] Furthermore, genetic factors for POF may be more complex as X;autosome translocations often disrupt no genes; therefore, other factors, such as position effects on autosomal genes, are proposed.[6] We had an opportunity to analyze four cases of POF each having t(X;autosome). Precise determination of translocation breakpoints in these patients may reveal direct evidence of POF-related genes and mechanisms of the formation of chromosomal translocations. Breakpoint sequences will be presented and discussed in relation to genes and formation process.

MATERIALS AND METHODS

Patients and genomic DNA preparation

A total of four POF patients with t(X;autosome) were recruited to this study. Case 1 had secondary amenorrhea and the other three (cases 2, 3 and 4) presented with primary amenorrhea. Cases 1, 3 and 4 are Japanese and case 2 is Caucasian. Case 2 was reported previously.[7] Chromosome analysis revealed 46,X,t(X;4)(q21.3;p15.2) in case 1, 46,X,t(X;2)(q22;p13) in case 2, 46,X,t(X;4)(q22.1;q12) in case 3 and 46,X,t(X;14)(q24;q32.1) in case 4. All translocations occurred *de novo*. In addition, 11 other POF patients were collected to check candidate gene abnormality. After informed consent was obtained, genomic DNA was prepared from peripheral blood leukocytes using QuickGene-610L (Fujifilm, Tokyo, Japan). Institutional review board approved the research protocol.

Fluorescence *in situ* hybridization

Metaphase chromosomes were prepared from peripheral blood lymphocytes of POF cases. Bacterial artificial chromosome DNA was labeled with fluorescein isothiocyanate- or Cy3-11-dUTP by Vysis Nick Translation kit (Vysis, Downers

[1]Department of Human Genetics, Yokohama City University Graduate School of Medicine, Yokohama, Japan; [2]Division of Neurology, Clinical Research Institute, Kanagawa Children's Medical Center, Yokohama, Japan; [3]Department of Cellular and Molecular Medicine, St George's University of London, London, UK; [4]Mater Pathology, Mater Health Services, Brisbane, Queensland, Australia; [5]Department of Medical Genetics, Shinshu University School of Medicine, Matsumoto, Japan; [6]Division of Obstetrics and Gynecology, Yokohama Municipal Citizens Hospital, Yokohama, Japan; [7]Department of Obstetrics and Gynecology and Reproductive Science, Yokohama City University Graduate School of Medicine, Yokohama, Japan and [8]Department of Radiology, Tokyo Metropolitan Kiyose Children's Hospital, Tokyo, Japan
Correspondence: Professor N Matsumoto, Department of Human Genetics, Yokohama City University Graduate School of Medicine, 3-9 Fukuura, Kanazawa-ku, Yokohama 236-0004, Japan.
E-mail: naomat@yokohama-cu.ac.jp
Received 17 September 2010; revised 10 November 2010; accepted 12 November 2010

Grove, IL, USA), and denatured at 70 °C for 10 min. Probe–hybridization mixtures (15 µl) were applied to chromosomes, incubated at 37 °C for 16–72 h, and then washed and mounted in antifade solution (Vector, Burlingame, CA, USA) containing 4′,6-diamidino-2-phenylindole. Photographs were taken on an AxioCam MR CCD fitted to Axioplan2 fluorescence microscope (Carl Zeiss, Oberkochen, Germany).

Southern blot and inverse PCR

Genomic DNA was digested with restriction enzymes: *Eco*RI and *Hin*dIII for case 1 and her parents, *Sac*I and *Eco*RI for case 2 and a normal female control, *Bam*HI and *Eco*RI for case 3 and her parents and *Nde*I and *Bgl*II for case 4 and her mother. Probes were made by PCR and labeled using DIG synthesis kit (Roche Applied Science, Basel, Switzerland). Hybridization, wash and detection were performed according to the manufacturer's protocol. Inverse PCR was performed using self-ligated DNA after digestion with *Eco*RI (cases 1 and 3), *Sac*I (case 2) and *Bgl*II (case 4). All the breakpoints were determined by sequencing inverse PCR products. Information of primers used is available on request.

Mutation analysis

Genomic DNA was obtained from peripheral blood leukocytes by standard methods and used for mutational screening. Protein coding exons of *COL4A6* (exons 1–45), insulin-like growth factor binding protein 7 (*IGFBP7*) (exons 1–5) and *C14orf159* (exons 4–16) were screened by high-resolution melt analysis using LightCycler 480 system II (Roche Applied Science, Tokyo, Japan), except for exon 1 of *IGFBP7*, which were analyzed by direct sequencing. PCR mixture contained 20 ng genomic DNA, 1× ExTaq buffer, 0.2 mM each dNTPs, 0.3 µM each primer, 0.25 µl SYTO9 (Invitrogen, Carlsbad, CA, USA) and 0.25 U ExTaq HS (Takara, Ohtsu, Japan). PCR was initially denatured at 94 °C for 2 min and cycled 45 times for 10 s at 94 °C, 15 s at 60 °C and 15 s at 72 °C, and then finalized at 72 °C for 1 min. High-resolution melt analysis was then performed. For exon 1 of *IGFBP7*, PCR mixture contained 20 ng genomic DNA, 1× GC buffer II, 0.4 mM each dNTPs, 1 µM each primers, 2% dimethylsulfoxide and 0.04 U LaTaq HS (Takara), and then PCR was initially denatured at 94 °C for 2 min and cycled 35 times at 94 °C for 20 s, at 60 °C for 20 s, at 72 °C for 1 min, and then finalized at 72 °C for 2 min. If a sample showed an aberrant melting curve pattern, the PCR product was purified using ExoSAP-IT (USB, Cleveland, OH, USA) and sequenced by a standard method using BigDye terminator ver.3 (Applied Biosystems, Foster City, CA, USA) on the ABI PRISM 3100 Genetic analyzer (Applied Biosystems). Sequences were compared with reference sequences using SeqScape version 2.7 (Applied Biosystems).

X-inactivation assay

Human androgen receptor assay and FRAXA locus methylation assay were performed as described previously,[8,9] with a slight modification. In brief, genomic DNA of patients, their parents and a female control was digested with two methylation-sensitive enzymes, *Hpa*II and *Hha*I. Subsequently, PCR was performed using digested and undigested DNA with human androgen receptor assay primers (FAM-labeled ARf: 5′-TCCAGAATCTGTTCCAGAG CGTGC-3′; ARr: 5′-CTCTACGATGGGCTTGGGGAGAAC-3′)[10] and FRAXA primers (FAM-labeled FRM1f: 5′-AGCCCCGCACTTCCACCACCAGCTCCT CCA-3′; FMR1r: 5′-GCTCAGCTCCGTTTCGGTTTCACTTCCGGT-3′), electrophoresed on ABI PRISM 3100 Genetic analyzer and analyzed with GeneMapper™ Software version 3.5 (Applied Biosystems).

RESULTS

Breakpoint sequences

Using fluorescence *in situ* hybridization analysis of metaphase chromosomes, we could identify Bacterial artificial chromosome clones spanning translocation breakpoints in each patient: RP11-636H11 at Xq22.3 (case 1), RP11-815E21 at Xq22.3 (case 2), RP11-589G9 at 4q12 (case 3) and RP11-904N19 at Xq24 (case 4). Southern blot analysis could identify aberrant bands in all the patients (Figure 1) and subsequent inverse PCR successfully cloned all breakpoints in the four cases. Breakpoint sequences are shown in Figure 2. Junction sequencing of der(X) and der(4) in case 1 revealed a 4192-bp deletion of chromosome X (UCSC genome browser coordinates March 2006 version: chr. X: 107 322 866–107 327 057 bp) and 7082-bp deletion (chr. 4: 11 846 359–11 853 387 bp) of chromosome 4, respectively. In addition, five unknown nucleotides were recognized at the der(X)

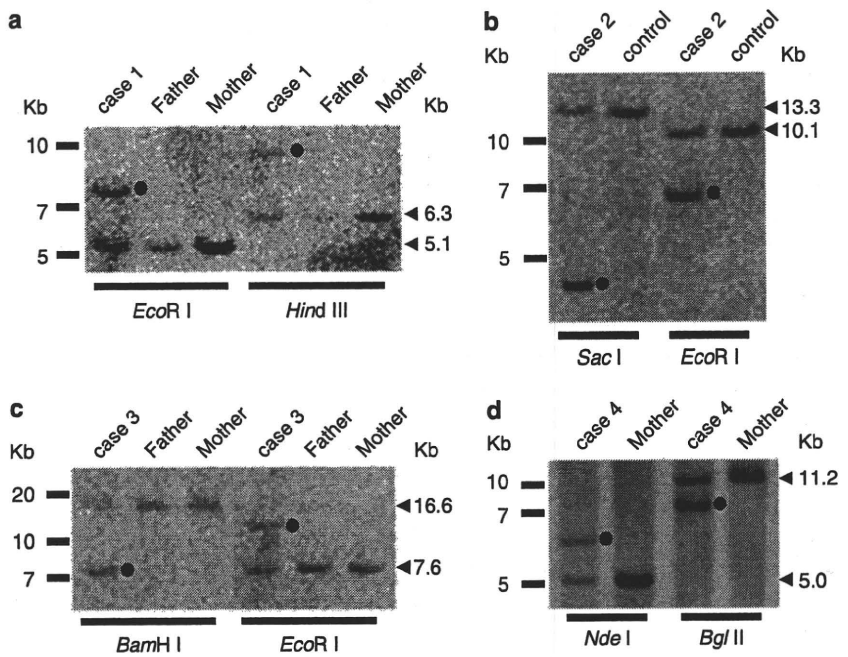

Figure 1 Southern blot analysis of four cases. (**a**) case 1, (**b**) case 2, (**c**) case 3 and (**d**) case 4. Aberrant bands are indicated with dots.

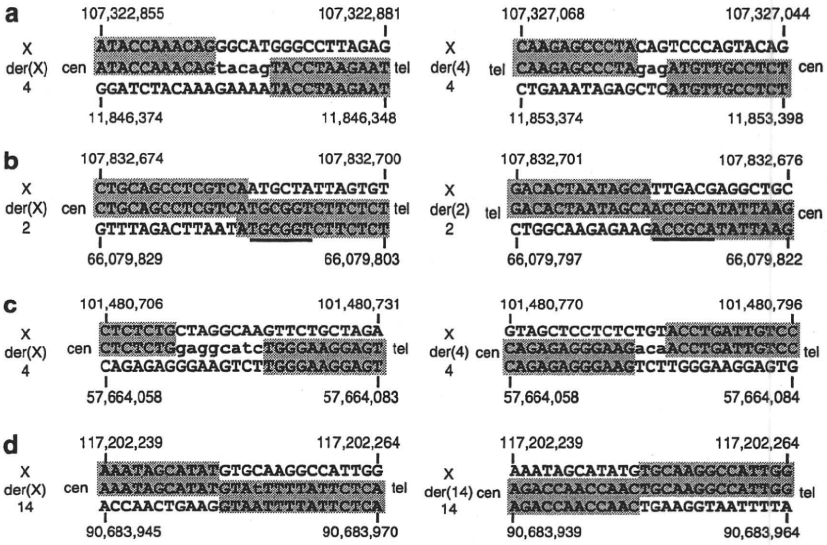

Figure 2 Breakpoint sequences of t(X;autosome) in four cases. (**a**) case 1, (**b**) case 2, (**c**) case 3 and (**d**) case 4. Top, middle and bottom sequences indicate those of normal X, derivative and normal autosomal chromosomes. Upper and lower cases indicate nucleotides of known and unknown origin, respectively. Matched sequences are with gray shadow. Underline indicates duplicated sequence. Numbers are based on the nucleotide position of the UCSC genome browser coordinates March 2006 version.

junction as well as three unknown nucleotides at der(4) (Figure 2a). Sequences of der(X) and der(2) in case 2 indicated six nucleotides (chr. 2: 66 079 810–66 079 816 bp) were duplicated (Figure 2b). In case 3, 71 nucleotides (chr. X: 101 480 713–101 480 782 bp) were deleted, and unknown eight nucleotides were inserted in der(X), and unknown three nucleotides were also recognized in der(4) (Figure 2c). In case 4, a nucleotide in chromosome X (chr. X: 117 202 250 bp) and five nucleotides in chromosome 14 (chr. 14: 90 683 951–90 683 955 bp) were missing (Figure 2d). The locations of X-chromosome breakpoints are shown in Figure 3. Translocation breakpoints disrupted *COL4A6* at Xq22.3 in case 1 (Figures 3a and b, Table 1), *IGFBP7* at 4q12 in case 3 (Table 1) and *C14orf159* at 14q32.12 in case 4 (Table 1). Other breakpoints did not involve any functional genes. Adjacent genes to breakpoints (less than 100 kb away) are *COL4A5* (5 kb away at Xq22.3) and *IRS4* (30 kb away at Xq22.3) in case 2, *NXF2* (12 or 21 kb away at Xq22.1) in case 3 and *KLHL13* (67 kb away at Xq24) in case 4 (Table 1). *COL4A6*, encoding collagen type IVα6, was the only disrupted X-linked gene in our POF patients.

X-inactivation assay

Human androgen receptor assay in cases 2 and 3 and FRAXA assay in cases 1 and 4 clearly indicated skewed X inactivation in all cases (100% in case 1, 94% in case 2, 98% in case 3 and 100% in case 4) and random patterns in their mothers available for this study (20–80%). Eleven other POF patients also showed random inactivation patterns (30–70%).

Mutation search

Considering accumulation of X-chromosome structural abnormalities in POF, X-chromosomal genes disrupted by rearrangements would be the primary target of this study. As *COL4A6* was completely disrupted in case 1 (Figure 3b), we started analyzing *COL4A6* as a candidate in 11 other POF patients. We found one heterozygous missense change, c.1460G>T (p.Gly487Val) (Figure 3c). This mutation was not recognized in 247 ethnically matched female controls (494 alleles). Web-based SIFT (http://sift.jcvi.org/) and PolyPhen (http://genetics.bwh.harvard.edu/pph/) did not indicate harmful effects of the amino-acid change on protein function: 0.26 by SIFT (predictable functional damage is <0.05) and 'benign' by PolyPhen, but the amino acid was evolutionally conserved (Figure 3d). The Gly487 was located between the (Gly–*X*–*Y*)*n* repeats. Parental origin of the change could not be confirmed as parental samples were unavailable. As *IGFB7* at 4q12 and *C14orf159* at 14q32.12 were also disrupted, both genes were analyzed in the 11 POF patients, but no mutation was found.

DISCUSSION

In this study, we could successfully determine the translocation breakpoints at nucleotide level in all the four cases analyzed. *COL4A6* at Xq22.3 in case 1, *IGFBP7* at 4q12 in case 3 and *C14orf159* at 14q32.12 in case 4 were disrupted. No genes were disrupted in case 2. Importantly, *COL4A6* was the only X-linked gene that was our primary target as a causative gene for POF. One missense change with benign nature outside the functional repeats was found in another POF patient who showed random X inactivation (35%).

In case 1, based on the skewing of X inactivation, der(X) should be active and normal X should be inactive. Thus, *COL4A6* is predicted to be functionally null in case 1 as the active allele is disrupted by the translocation. Collagen type IV is an essential component of basement membrane, consisting of six distinct α-chains (α1–α6) encoded by *COL4A1* to *COL4A6*. These six genes are located in three pairs with head-to-head orientation, *COL4A1*/*COL4A2* on chromosome 13, *COL4A3*/*COL4A4* on chromosome 2 and *COL4A5*/*COL4A6* on chromosome X. The chains interact and assemble with specificity to form three distinct patterns: α1α1α2, α3α4α5 and α5α5α6.[11] The α5- and α6-chains are found in the basement membrane of skin, smooth muscle and kidney.[12] Two transcripts of *COL4A6* are known, isoforms A and B (Figure 3b). The protein structure of collagen type IV contains an amino-terminal collagenous domain (also called 7S domain), a triple-helical region (Gly–*X*–*Y*) and a carboxyl-terminal

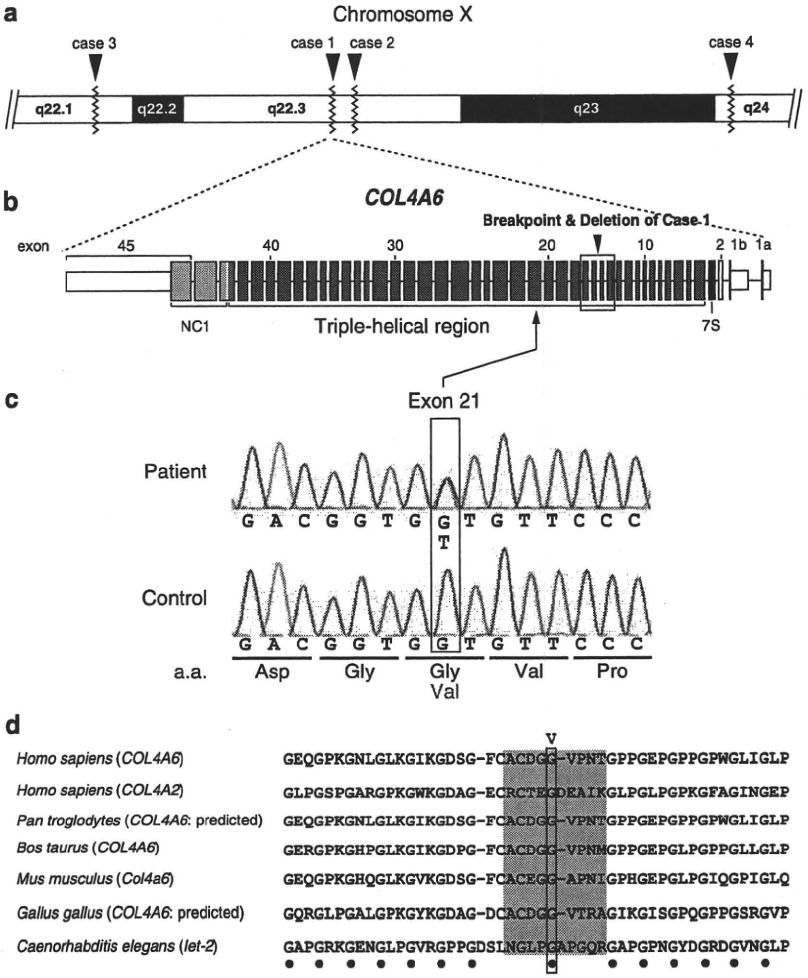

Figure 3 Location of the X-chromosome breakpoints and the *COL4A6* gene. (**a**) Breakpoint locations (zigzag lines) of four cases around Xq22.1–q24. (**b**) Schema of the *COL4A6* gene. Boxes are exons with numbering. White, dark gray, gray and light gray boxes indicate UTRs, 7S domain, triple-helical region and non-collagenous (NC1) domain, respectively. Breakpoint of the translocation with associated deletion is shown above boxes. (**c**) Heterozygous missense mutation, c.1460G>T (p.Gly487Val) at exon 21, is shown in the upper panel and wild-type sequence is shown in the lower panel. a.a.: amino acid. (**d**) Evolutionary conservation of the Gly487. CLUSTALW (http://align.genome.jp/) was used for this analysis. Dots show perfect conservation. Gray box is a space between the Gly–*X*–*Y* repeats.

Table 1 Genes within a 100-kb distance from translocation breakpoints

Case	*Chromosome X*	*Autosome*
1	*COL4A6*	None
	[q22.3]	[4p15.33]
2	*COL4A5* (5 kb)	None
	IRS4 (30 kb)	[2p14]
	[q22.3]	
3	*NXF2*[a] (12 or 21 kb)	*IGFBP7*
	[q22.1]	[4q12]
4	*KLHL13* (67 kb)	*C14orf159*
	[q24]	[14q32.12]

Round and square brackets indicate a distance from a breakpoint and chromosomal location, respectively.
Underlined genes are disrupted by breakpoints.
[a]*NXF2* is mapped to two adjacent segmental duplications.

non-collagenous (NC1) domain (Figure 3b).[13] We found a missense change, c.1460G>T (p.Gly487Val), in exon 21 in another POF patient (Figure 3c). Although this change is not found in 247 Japanese controls, its benign nature is suspected based on the web-based programs, the location outside the functional repeats and random X inactivation leading to the production of normal α6-chain. Parental samples were unfortunately unavailable to test the origin of the nucleotide change.

COL4A6 abnormality is known to be related to Alport syndrome with diffuse leiomyomas (AL-DS). *COL4A6* deletions in AL-DS are limited to exons 1, 1′ and 2 always together with *COL4A5* deletion in diverse extent.[14,15] In this paper, we first describe a POF patient (case 1) with disruption of only *COL4A6* not involving *COL4A5*. The inactivated normal X chromosome as well as the der(X) with disrupted *COL4A6* should lead to functionally null status in the patient. Extracellular matrix proteins (including COL4A6) have been shown to alter Leydig cell steroidogenesis *in vivo*, implying that Leydig cell steroidogenic